The age and origin of cratonic lithospheric mantle: Archean dunites vs. Paleoproterozoic harzburgites from the Udachnaya kimberlite, Siberian craton

Dmitri Ionov, Zhe Liu, Jie Li, Alexander Golovin, Andrey Korsakov, Yigang
Xu

1 **The age and origin of cratonic lithospheric mantle: Archean**

2 **dunites vs. Paleoproterozoic harzburgites from the Udachnaya**

3 **kimberlite, Siberian craton**

4

5 Dmitri A. Ionov[a,b*], Zhe Liu[a], Jie Li[a], Alexander V. Golovin[c], Andrey V. Korsakov[c], Yigang

6 Xu[a]

7

8 [a] *State Key Laboratory of Isotope Geochemistry, Guangzhou Institute of Geochemistry,*

9 *Chinese Academy of Sciences, 510640 Guangzhou, China*

10 [b] *Géosciences Montpellier, University of Montpellier, 34095 Montpellier, France*

11 [c] *V.S. Sobolev Institute of Geology and Mineralogy, Siberian Branch, Russian Academy of*

12 *Sciences and Novosibirsk State University, Novosibirsk 630090, Russia*

13

14

15

16

17 ∗ *Corresponding author; e-mail: dionov@umontpellier.fr, phone: +33 (0)467143349*

18

19 *11996 words in the main text*

20

21   ABSTRACT *(485words)*

22   Cratonic lithospheric mantle is believed to have been formed in the Archean, but kimberlite-

23   hosted coarse peridotites from Udachnaya in the central Siberian craton typically yield

24   Paleoproterozoic Re-depletion Os isotope ages (T_{RD}). By comparison, olivine megacrysts

25   from Udachnaya, sometimes called "megacrystalline peridotites", often yield Archean T_{RD}

26   ages, but the nature of these rare materials remains enigmatic. We provide whole-rock (WR)

27   Re-Os isotope and PGE analyses for 24 olivine-rich xenoliths from Udachnaya as well as

28   modal and petrographic data, WR and mineral major and trace element compositions. The

29   samples were selected based on (a) high olivine abundances in hand specimens and (b)

30   sufficient freshness and size to yield representative WR powders. They comprise medium- to

31   coarse-grained (olivine <1 cm) dunites, a megacrystalline (olivine >1 cm) dunite, olivine

32   megacrysts and low-orthopyroxene (11–21% opx) harzburgites equilibrated at 783–1154°C

33   and 3.9–6.5 GPa; coarse dunites have not been previously reported from Udachnaya; two

34   xenoliths contain ilmenite. The harzburgites and dunites have similar WR variation ranges of

35   Ca, Al, Fe, Cr and Mg# (0.917–0.934) typical of refractory cratonic peridotites, but the

36   dunites tend to have higher MgO, NiO and Mg/Si. Mineral abundances and those of Ca and

37   Al are not correlated with $Mg\#_{WR}$; they are not due to differences in melting degrees but are

38   linked to metasomatism. Several samples with high $^{187}Re/^{188}Os$ show a positive linear

39   correlation with $^{187}Os/^{188}Os$ with an apparent age of 0.37 Ga, same as eruption age of host

40   kimberlite. Robust T_{RD} ages were obtained for 16 xenoliths with low $^{187}Re/^{188}Os$ (0.02–0.13).

41   T_{RD} ages for low-opx harzburgites (1.9–2.1 Ga; average 2.0 ± 0.1 Ga) are manifestly lower

42   than for dunites and megacrysts (2.4–3.1 Ga); the latter define two subsets with average T_{RD}

43   of 2.6 ± 0.1 Ga and 3.0 ± 0.1 Ga, and T_{MA} of 3.0 ± 0.2 Ga and 3.3 ± 0.1 Ga, respectively.

44   Differences in olivine grain size (coarse vs. megacrystalline) are not related to age. The age

45   relations suggest that the dunites and megacrysts could not be produced by re-melting of

46 harzburgites, e.g. in arc settings, nor be melt channel materials in harzburgites. Instead, they

47 are relict fragments of lithospheric mantle formed in the Archean (likely in two events at or

48 after 2.6 Ga and 3.0 Ga) that were incorporated into cratonic lithosphere during the final

49 assembly of the Siberian craton in the Paleoproterozoic. A multi-stage formation of the

50 Siberian lithospheric mantle is consistent with crustal basement ages from U-Pb dating of

51 zircons from crustal xenoliths at Udachnaya and detrital zircons from the northern Siberian

52 craton (1.8–2.0, 2.4–2.8 and 3.0–3.4 Ga). The new data from the Siberian and other cratons

53 suggest that the formation of strongly melt-depleted cratonic lithosphere (e.g. Mg# $\geq$0.92) did

54 not stop at the Archean-Proterozoic boundary as is commonly thought, but continued in the

55 Paleoproterozoic. The same may be valid for the transition from the 'Archean' (4–2.5 Ga) to

56 modern tectonic regimes.

57

1. Introduction

1.1. *Formation stages of the Siberian craton*

Cratons are the oldest parts of continents. Essential components of their crustal basement are Archean (>2.5 Ga) magmatic and metamorphic rocks with widespread ~2.7 Ga and older ages (e.g. Condie, 2014). The only robust dating methodology for refractory peridotites, the main components of cratonic mantle, is based on the Re-Os isotope system because Os is highly compatible during mantle melting. These rocks do not normally show isochrone relations (e.g. Rudnick and Walker, 2009), but their formation can be traced back using model "Re-depletion" ages (T_{RD}) assuming that all Re was extracted from pristine mantle in a single, high-degree ($\geq$30%) melting event (Walker et al., 1989). The T_{RD} method was defined for whole-rock (WR) peridotite xenoliths, and initially applied to analytical samples from the Kaapvaal and Siberian cratons prepared from large amounts (hundreds of grams) of material required to bridge modal heterogeneities in coarse-grained rocks and thus provide representative compositional data (Boyd et al., 1997; Pearson et al., 1995b; Walker et al., 1989). The T_{RD} values for individual samples have high uncertainties, and it is common to constrain lithospheric formation ages based on either peaks on T_{RD} frequency distribution plots or the oldest ages whereas dispersed younger T_{RD} values are more likely to be due to more recent melt metasomatism (e.g. Carlson et al., 1999; Irvine et al., 2003).

Rhenium-osmium isotope data on coarse (low-T) WR peridotites show that the lithospheric mantle beneath several well-studied cratons in North America and South Africa formed in the Archean, with T_{RD} distribution peaks at 2.6 to 2.8 Ga (e.g. Carlson et al., 2005; Wittig et al., 2010b). The similar crust and mantle formation ages (crust-mantle coupling, (e.g. Pearson et al., 1995a)) are two related facets of lithosphere development, i.e. melt extraction from fertile mantle yields both refractory residues that form lithospheric mantle and mafic melts that form cratonic proto-crust (Herzberg and Rudnick, 2012; Moyen et al., 2017).

4

85   The formation (melt extraction) age for the lithospheric mantle of the Siberian craton,

86   however, continues to be debated. Peridotite xenoliths suitable for Re-Os dating are available

87   almost exclusively from two kimberlite pipes: Udachnaya in the center of the craton and

88   Obnazhennaya near its northeastern (NE) margin (KML file). Published T_{RD} estimates for

89   WR refractory peridotites from both pipes are puzzling because they show bimodal

90   distribution with peaks at ~2.0 Ga and 2.8 Ga (Ionov et al., 2015a). The pioneering work of

91   Pearson et al. (1995b) provided T_{RD} values for 16 olivine-rich xenoliths from Udachnaya

92   including four Archean (2.6–3.2 Ga) and eight Paleoproterozoic (1.7–2.2 Ga) ages, as well as

93   four younger (0.9–1.4 Ga) values attributed to metasomatism. Pearson et al. (1995b) argued

94   for an Archean (≥3.2 Ga) formation age for the Siberian craton mantle and downplayed the

95   Paleoproterozoic T_{RD} values, in spite of their greater numbers. For instance, they speculated

96   that the Archean materials may be located deeper in the lithosphere than the Paleoproterozoic

97   peridotites.

98   Later work, by contrast, found mainly Paleoproterozoic ages for a range of mantle samples

99   from Udachnaya. Ionov et al. (2015b) reported Re-Os isotope data for 29 WR peridotites and

100   obtained ~2 Ga T_{RD} values for the majority of coarse refractory rocks (Mg# 0.92–0.93), which

101   they viewed as pristine melting residues, as well as generally lower (0.9–2.0 Ga) estimates for

102   deformed, low-Mg# (0.907–0.919) garnet peridotites they ascribed to the effects of melt

103   metasomatism on 2 Ga old residues. Doucet et al. (2015) obtained ~1.8 Ga model Hf-Nd

104   isotope ages for spinel harzburgites from the same suite while Wiggers de Vries et al. (2013)

105   reported ~1.8 Ga T_{RD} ages for sulfide inclusions in diamonds. Peridotite xenoliths from the

106   Obnazhennaya kimberlite, by comparison, show both Archean and Paleoproterozoic ages

107   (peaks at 2.8 and 1.9 Ga), with no relation to their modal (dunites or harzburgites) or WR

108   major element compositions (Ionov et al., 2015a). Likewise, Moyen et al. (2017) reported a

109   bimodal age distribution for crustal xenoliths from Udachnaya (~1.9 Ga for the lower crust

and ~2.8 and for the upper crust) and suggested that the Siberian cratonic lithosphere formed

in two stages, i.e. first in the Archean, then in the Paleoproterozoic when much of the pre-

existing lithospheric mantle and lower crust was replaced with younger melting residues.

An alternative approach to dating Udachnaya peridotites was employed by Pernet-Fisher et

al. (2015) who reported Re-Os isotope data not on representative WR samples, but on small

amounts of material extracted from five xenoliths and on olivine separates from another five

xenoliths. The advantages of such an approach are that small xenoliths are easier to find and

handle, yet, the absence of modal and WR chemical data, that are essential to assess the

melting and metasomatism history of the mantle, adds uncertainties to age estimates and their

interpretation. Pernet-Fisher et al. (2015) obtained T_{RD} values from ≤0 to 2.7 Ga and argued

that they record melt extraction events ranging from ~3 Ga to ~1.2 Ga despite strong evidence

(common deformation, low olivine Mg# (0.894–0.914) and high Re/Os ratios) for melt

metasomatism evoked for such samples in earlier studies of Udachnaya xenoliths (Agashev et

al., 2013; Ionov et al., 2015b; Pearson et al., 1995b). Finally, Pernet-Fisher et al. (2019)

reported Archean T_{RD} values for fragments of seven (out of eleven analysed) olivine

megacrysts from Udachnaya (apparently similar to those analysed by Pearson et al. (1995b)).

To sum up, three formation models have been proposed for the mantle lithosphere of the

Siberian craton: (1) overall Archean (≥3 Ga) formation age (Pearson et al., 1995b; Pernet-

Fisher et al., 2019), (2) continuous or multi-stage formation from the Eoarchean to

Mesoproterozoic (Pernet-Fisher et al., 2015), and (3) a two-stage formation based on bimodal

age distribution for mantle and crustal rocks (Ionov et al., 2015b; Moyen et al., 2017).

1.2. *The enigmatic nature of the oldest materials in the Siberian cratonic mantle*

The nature of the rare mantle materials with Archean ages from Udachnaya remains

enigmatic. Textural, modal, chemical and isotopic features of such xenoliths, and their

135 differences with younger rocks, must be constrained to gain insights into the earliest stages of

136 lithospheric formation in the central Siberian craton. Pearson et al. (1995b) referred to three

137 out of four of their Archean samples as "megacrystalline peridotites", for which only

138 qualitative descriptions and mineral analyses were reported. Their $Mg\#_{ol}$ [$Mg/(Mg+Fe)_{at}$ of

139 olivine] (0.922–0.927) fall in the range for coarse harzburgites from Udachnaya (0.919–

140 0.930) with ~2 Ga T_{RD} ages (Doucet et al., 2013; Ionov et al., 2015b); some contain rare sub-

141 calcic garnets (Pokhilenko et al., 1991; Sobolev et al., 1984), but published data are too scarce

142 to assess links of Archean ages with garnet compositions. Another Archean sample, spinel

143 peridotite UV191/89 (Pearson et al., 1995b) was reported to contain 12% orthopyroxene

144 (opx), but is referred to as dunite (Boyd et al., 1997).

145   Pearson et al. (1995b) linked the Archean ages chiefly to "megacrystalline peridotites"

146 (probably, olivine megacrysts), but the absence of petrographic descriptions and quantitative

147 data on modal or bulk chemical compositions of these samples renders it difficult to constrain

148 their origin and compare them to other mantle xenoliths. Sobolev et al. (1984) collected ~300

149 olivine megacrysts and what they call "megacrystalline dunites" at Udachnaya. Most of them

150 are very small (1–3 cm), with few samples >5 cm in at least one dimension; the largest olivine

151 grains measure ~10 cm, but their size varies both within and between the samples, and grades

152 to <1 cm. The megacrystalline olivine may contain inclusions of garnet (mainly Ca-poor, Cr-

153 rich), less commonly, Cr-spinel, opx, clinopyroxene (cpx) and ilmenite, i.e. minerals also

154 common in coarse peridotites. Pernet-Fisher et al. (2019) used He-Os isotope and trace

155 element data for olivine megacrysts from Udachnaya to examine their metasomatism but did

156 not address the origin of these exotic materials (especially, how they could be produced by

157 melt extraction) or their relations with coarse harzburgites.

158   A particular problem is ambiguous terminology and sample descriptions in the previous

159 studies. Pernet-Fisher et al. (2019) described each of their samples as "one large megacryst"

160 of olivine (mainly ≤2–3 cm in size), yet also called them "megacrystalline dunites", a term

161 appropriate for rocks composed of aggregates of olivine grains, but questionable for single

162 olivine crystals. For instance, kimberlites at Udachnaya and elsewhere commonly contain

163 large mantle-derived clinopyroxene crystals (Abersteiner et al., 2019), but they are not

164 referred to as "megacrystalline pyroxenites". "Megacrystalline dunites" analyzed by Pearson

165 et al. (1995b) may rather be olivine megacrysts as well, i.e. essentially the same kind of

166 materials as those reported later by Pernet-Fisher et al. (2019).

167   Overall, it is not clear what distinguishes these Archean materials from post-Archean

168 spinel and garnet peridotites from Udachnaya: their ultra-coarse grain size, their high modal

169 olivine or other parameters. It appears that Archean T_{RD} ages for Udachnaya have been so far

170 obtained almost exclusively on olivine megacrysts. This also raises a question whether the

171 Udachnaya-East kimberlites enclose any normal dunites, i.e. poly-grain olivine-rich rocks

172 similar in grain size to other peridotite xenoliths, like dunites in the Obnazhennaya kimberlite

173 (Ionov et al., 2015a).

174

175 1.3. *Objectives of this study*

176   Given the limited number of samples studied and the dearth of petrologic and chemical

177 WR data reported (Pearson et al., 1995b; Pernet-Fisher et al., 2019), the nature of Archean

178 mantle materials from Udachnaya, in particular of the megacrystalline xenoliths and coarse

179 olivine-rich peridotites, remains to be fully established. To address the unresolved questions,

180 we collected and studied olivine-rich Udachnaya peridotites regardless of their grain size,

181 sufficiently large to yield representative WR powders. Robust modal, WR chemical data and

182 formation ages for these potentially oldest lithospheric mantle materials in Siberia, including

183 ultra-coarse-grained xenoliths, are essential to constraining their origin, notably melting

184 history in relation to relevant experimental data (e.g. Herzberg, 2004; Walter, 2003).

185   Here we provide the first comprehensive set of petrologic, geochemical and age data for

186   main types of the most refractory xenolith materials in kimberlites from the Siberian craton:

187   dunites (including their "megacrystalline" variety) and olivine-rich harzburgites, as well as

188   large olivine megacrysts reported in earlier studies (Pearson et al., 1995b; Pernet-Fisher et al.,

189   2019). We report highly siderophile element (HSE) concentration data and Os isotopic

190   compositions for 24 new, olivine-rich peridotites, as well as three opx-rich xenoliths, from the

191   Udachnaya kimberlite together with modal and petrographic data, bulk-rock and mineral

192   major and trace element compositions. The major objectives of this paper are to: (a) establish

193   the Os isotope and HSE distribution in these materials; (b) better constrain their formation

194   (melt extraction) ages, and (c) examine relations between the mantle and crustal components

195   of different ages during the formation and assembly of the central Siberian craton.

196

197   **2. Geological setting and samples**

198   2.1. *Geologic setting of the Udachnaya pipe*

199   The Udachnaya kimberlite (66°26'N, 112°19'E) is located in the Sakha (Yakutia) Republic

200   of the Russian Federation, close to the center of Siberia (KML file). It belongs to the Daldyn-

201   Alakit field in the southwestern portion of the Yakutian kimberlite province that extends from

202   the center to northern and NE parts of the Siberian craton (KML file). The kimberlite was

203   mined for diamonds in an open pit in 1971–2015. From 2015, the mining and crushing have

204   been done underground making it unlikely for more xenoliths to be recovered. Samples in this

205   study were collected at ~400–640 m depth near the center of the Udachnaya-East pipe in

206   remarkably well-preserved type-I kimberlite (Kamenetsky et al., 2012) or in the storage area

207   of mined materials from the same depth range. They are generally less altered than samples

208   found near the surface or at shallow levels in the mine (e.g. Boyd et al., 1997; Pearson et al.,

209   1995b).

210   The pipe is hosted by Neoproterozoic to Paleozoic sedimentary rocks, and is believed to be

211   located in the Daldyn block of the craton. This block is exposed on the Anabar shield north of

212   Udachnaya, where crustal rocks have U-Pb zircon ages from 1.8 to 3.4 Ga with three main

213   periods: 1.8–2.0 Ga, 2.4–2.8 Ga and 3.0–3.4 Ga (Paquette et al., 2017). U-Pb dating of

214   perovskite in kimberlite yielded an eruption age of 367±5 Ma for the Udachnaya-East pipe

215   and a range from 353±5 to 361±4 Ma for the adjacent Udachnaya-West as well as several

216   other pipes in the Daldyn field (Kinny et al., 1997). Other estimates range from 347 to 429

217   Ma (see Ionov et al. (2015b)). For simplicity, and in line with some previous peridotite

218   xenolith studies (e.g. Ionov et al., 2015b), we assume below an eruption age of 360 Ma.

219   Previous work has provided much information about the Udachnaya kimberlite and its

220   various xenolithic materials (Abersteiner et al., 2018; Agashev et al., 2013; Golovin et al.,

221   2018; Jean et al., 2016; Kamenetsky et al., 2014; Kamenetsky et al., 2012; Kamenetsky et al.,

222   2008; Kitayama et al., 2017; Pernet-Fisher et al., 2019; Sobolev et al., 2009; Spetsius and

223   Serenko, 1990). Multi-discipline studies of a suite of large, fresh peridotite xenoliths from

224   Udachnaya have provided comprehensive data on their petrography and chemical

225   composition (Doucet et al., 2013; Doucet et al., 2012; Doucet et al., 2014; Goncharov et al.,

226   2012; Ionov et al., 2010), radiogenic and stable isotopes (Doucet et al., 2016; Ionov et al.,

227   2017; Kang et al., 2017; Xia et al., 2017) as well as petrophysical properties (Bascou et al.,

228   2011) that address melt extraction and metasomatism during the formation and evolution of

229   the cratonic lithosphere.

230

231   2.2. *Sample selection and preparation*

232   Olivine-rich xenoliths, including olivine megacrysts and "megacrystalline dunites" ≥5 cm

233   in size were targeted in the field in recent years, but they are very scarce and usually hard to

234   recover from massive kimberlites in Udachnaya. In addition, hundreds of xenoliths collected

235   by AVG and AVK since 2003 were re-examined to select olivine-rich (≥80%) samples,

236   regardless of their grain size. Twenty-four such xenoliths (including U220 earlier reported by

237   Ionov et al. (2010)) were chosen for this study based on their size, low alteration degrees and

238   high modal olivine (from visual inspection) without preference for any rock type. Three opx-

239   rich rocks were included as well for comparison. The samples are listed in Table 1, which

240   provides a summary of essential data for each xenolith; the full dataset is given in Electronic

241   Supplement 1 (ES1).

242   The xenoliths ranged in size from 5 to 20 cm. It may not be certain if some very coarse-

243   grained samples 5–10 cm in size are large enough to prepare representative WR powders, but

244   they appear to be the largest samples currently available for these rare rock types, and no

245   larger xenoliths from Udachnaya may be accessible in the future. Their rinds were removed

246   by hammer or by sawing if they contained kimberlite or alteration products; sawn surfaces

247   were cleaned on alumina disks. Material from xenolith cores (32–250 g and an ilmenite-

248   bearing sample of 16 g; Table 1) was inspected to make sure it contained no veins or modal

249   gradations and crushed to <5–10 mm in a jaw crusher with ceramic jaws and inner walls.

250   Photographs of WR samples prepared for crushing are given in Electronic Supplement 2

251   (ES2). Splits of crushed material (10–20 g) were ground to fine powder in agate. The crusher

252   and jars (see photos in ES2) were carefully cleaned to avoid cross-contamination.

253

254   **3. Methods**

255   Detailed descriptions of the methods are provided in ES3.

256   3.1. *Major elements, modal compositions and P-T estimates*

257   Whole rock major element compositions were obtained by wavelength-dispersive (WD) X-

258   ray fluorescence (XRF) spectrometry at J. Gutenberg University, Mainz. Rock powders were

259   ignited for ≥3 h at 1000°C to turn all FeO into Fe_2O_3, expel volatiles, and measure the loss on

ignition (LOI). Glass beads, produced by fusing 0.8 g of ignited powders with 4.8 g of dried

LiB$_4$O$_7$ (1:7 dilution) were analyzed on a Philips PW 1404 spectrometer using ultramafic and

mafic reference samples as external standards. Peridotite reference samples JP-1 and UBN

were analyzed as unknowns to control accuracy with results close to recommended values

(ES1). The compositions are reported with Fe$_2$O$_3$ recalculated to FeO.

Minerals were analyzed for major elements by WD electron probe microanalysis (EPMA)

at the Guangzhou Institute of Geochemistry, Chinese Academy of Sciences (GIG-CAS) in

grain mounts. Garnet and spinel were run on a JXA-8900 instrument at 20 kV accelerating

voltage, 40 nA beam current, 1–3 mm beam diameter, counting times of 20–40 s for peaks

and 20–40 s for background (Ziberna et al., 2016) with ZAF data reduction procedure.

Olivine and pyroxenes (homogeneous cores delimited using BSE imaging) were analyzed on

Cameca SXFive FE. Olivine was run at 20 kV, 20–60 s peak counting time, and the current of

20 nA and 100 nA. Data obtained at 20nA are reported for Si, Fe, Mn and Ni, and data at 100

nA for Cr, Ca and Na; concentrations of Al and Ti are below detection for nearly all samples.

Machine drift and accuracy were monitored with the MongOl reference sample (Batanova et

al., 2019), see ES3. Pyroxenes were run at 20 kV, 40 nA, 1–3 mm beam, and 40 s counting

times for peaks and background; the PAP procedure was used for matrix correction.

Equilibration temperatures (T) were calculated based on the following mineral pairs and

methods depending on the minerals present: (a) cpx-opx (Taylor, 1998); (b) Ca-in-cpx (Nimis

and Taylor, 2000); (c) Ca-in-opx (Brey and Köhler, 1990) corrected as in Nimis and Grütter

(2010); (d) opx-garnet (Nimis and Grütter, 2010). Equilibration pressure was estimated with

opx-garnet barometer of Nickel and Green (1985); for spinel peridotites it was evaluated

based on projection of their equilibration T's to local geotherm (Goncharov et al., 2012), and

for garnet peridotites using P values for samples with similar T's.

Modal abundances were calculated from a least-squares fit of the WR major element

285 composition to its constituent minerals. The method chooses predicted values of modal

286 abundances that minimize the sum of squared errors of prediction values for WR abundances

287 of Si, Ti, Al, Cr, Fe, Mn, Mg, Ca, Na and Ni based on EPMA data for minerals compared to

288 actual WR values for these elements. The totals of the calculated modal abundances are

289 within ±0.5% of 100% for 16 xenoliths out of 27, ±0.9% for 25 xenoliths and within ±1.2%

290 for pyroxenite 194-13 and ilmenite-bearing dunite 571-13 (ES1), possibly due to the presence

291 of unidentified accessory minerals. The modal estimates are reported in Table 1 normalized to

292 yield 100% totals. The same software has been used in our mantle xenolith studies in the last

293 two decades. Ionov et al. (2010) calculated modal compositions for three Udachnaya

294 peridotites reported by Boyd et al. (1997) using their data and the same software as in this

295 study. They reproduced four of the six modal olivine and opx values from Boyd et al. (1997)

296 within 0.1%, and obtained lower opx values (by 0.8 and 1.5%) in two samples. Overall, the

297 uncertainties of our modal estimates for olivine and opx appear to be within ±1.5%.

298

299 3.2. *Lithophile trace elements*

300   Trace elements in WR powders were determined by inductively-coupled plasma (ICP)

301 mass-spectrometry (MS) at the GIG-CAS. A multi-stage acid-digestion procedure in bombs

302 was employed for complete dissolution of acid-resistant phases like spinel and ilmenite (ES3).

303 Samples in 3% HNO_3 (1:4000 dilution) spiked with a Rh-Re solution to correct for mass-

304 related instrument drift were analyzed on a Thermo-Scientific iCAP Q with USGS reference

305 materials (BHVO-2, GSR-1, GSR-2, GSR-3, AGV-2, W-2a, SARM-4) for calibration; oxide

306 yields were <3% based on the $^{140}Ce^{16}O/^{140}Ce$ ratio. USGS basalt BIR-1 was repeatedly

307 measured as unknown and yielded abundances within ≤6% of reference values and

308 reproducibility ≤10% (2 RSD, relative standard deviation) for most elements (ES 1).

309   Trace elements in minerals were analyzed at the GIG-CAS in polished grain mounts by

310 laser ablation (LA) ICPMS with a sector field ELEMENT XR (Thermo Fisher Scientific)

311 coupled with a 193-nm (ArF) Resonetics RESOlution M-50 laser (6Hz, 4 J cm^{-2}, beam 45

312 μm). Calibration was done with USGS glasses BCR-2G, BHVO-2G and GSD-1G (external

313 standards), and Si as internal standard. Thirty analyses of TB-1G yielded abundances within

314 ≤8% of reference values and reproducibility of ≤10% (2 RSD) for most elements (ES1).

315

316 3.3. *Os isotope and HSE analyses of whole-rocks at the GIG-CAS*

317   Os isotope ratios and Re and Os abundances were determined in ~1 g of powder aliquots.

318 The samples were mixed with a ^{185}Re-^{190}Os spike, sealed into Pyrex Carius tubes with 10 ml

319 of inverse aqua regia (3:1 HNO_3:HCl) and kept at 240°C for 2 days. Osmium was extracted

320 from the aqua regia to CCl_4, then to HBr, micro-distilled using CrO_3-4N H_2SO_4, then loaded

321 onto Pt filaments and followed when dry with a $Ba(OH)_2$ activator. Os isotopic ratios were

322 measured on a Triton thermal ionization MS (TIMS) via peak hopping on single electron

323 multiplier. Data were fractionation-corrected to $^{192}Os/^{188}Os$ = 3.08271. Total Os blank was

324 0.46 ± 0.42 (2σ, n=5) pg. A mean $^{187}Os/^{188}Os$ of 0.12042 ± 0.00027 (2 σ, n=6) was obtained

325 for Merck Chemical AA standard solution for the period of analysis. These results are in good

326 agreement with a value of 0.12022 ± 0.00020 (2σ, n=14) measured on the same mass

327 spectrometer in Faraday cup mode (Li et al., 2010). Zhang et al. (2017) found no systematic

328 differences in Os isotope ratios for USGS BIR-1a digested in Carius tubes either with or

329 without de-silicification with HF prior to Carius tube digestion, indicating that an HF

330 dissolution step is not required to obtain reliable Re-Os isotope results. Our mean $^{187}Os/^{188}Os$

331 value of 0.13373±0.00081 (2σ, n=5) for BIR-1a analyzed with the same procedure is in good

332 agreement with published data (0.13372 ± 0.00080 and 0.13371± 0.00092) reported by

333 Ishikawa et al. (2014) and Zhang et al. (2017), respectively.

334   The aqua regia was dried and re-dissolved in 1N HCl after Os extraction; Re was separated

335   by anion chromatography (see ES3), with a cleanup column to exclude interferences. Its

336   concentrations were measured by isotope dilution (ID) ICP-MS on a Thermo-Scientific

337   XSERIES. Total Re blank was 6.3 ± 1.1 (2σ, n = 5) pg.

338   A separate aliquot of rock powder was used for PGE analyses. The concentrations of Ir,

339   Ru, Pt and Pd were determined by ID-ICPMS after Carius tube digestion (see above) with a

340   mixed spike containing enriched isotopes of these elements in the correct proportions for a

341   rock with chondritic PGE ratios. Purified solutions of these elements were obtained using

342   cation columns (see ES3) and analyzed on a Thermo Scientific iCAP-Q. Total procedural

343   blank was <5 pg for Ir, 13 pg for Ru, 17 pg for Pd and 28 pg for Pt. Values for each element

344   are averages of nine replicate analyses, with RSD <10% in most cases. The concentrations

345   obtained for peridotite standards GPT-3 and GPT-4 (Chinese national reference materials

346   GBW07290 and GBW07291) are within error of recommended values (ES3).

347

348   **4. Results**

349   4.1. *Petrography and modal composition*

350   Among 27 samples in this study, four are olivine megacrysts, eleven are dunites (rocks

351   with ≥90% olivine as multiple grains), another eleven are harzburgites (52–87% olivine) and

352   one is olivine orthopyroxenite (Streckeisen, 1976). The samples are further subdivided into

353   four groups based on modal abundances and microstructures (Table 1; Fig. 1; ES1-2).

354   (1) Five megacrystalline xenoliths are distinguished by very coarse grain size of olivine

355   (>1 cm). Four of them look like individual olivine crystals (megacrysts) that may contain

356   inclusions of opx, cpx, garnet and spinel, e.g. U220 >8 cm long and >100 g in weight (Fig.

357   1b). They are comparable to seven "group 1" (Mg#$_{Ol}$ >0.92) Udachnaya xenoliths reported by

358   Pernet-Fisher et al. (2019), each described as "one large megacryst" of olivine, and apparently

359   also to three samples that Pearson et al. (1995b) called "megacrystalline dunites", but are

360 likely olivine megacrysts as well. One of our megacrystalline samples (Uv83-13) is an

361 aggregate of very large (>1 cm) olivine and small interstitial grains of pyroxenes, garnet and

362 spinel, i.e. could be called megacrystalline dunite (rock composed primarily of olivine grains).

363   (2) Nine "coarse dunites" (Fig. 1c-f) have protogranular microstructure and consist of

364 olivine grains 1–5 mm in size and smaller interstitial pyroxenes, garnet and spinel; sample

365 571-13 contains ~3% of purple ilmenite coexisting with garnet. Some contain clusters rich in

366 garnet, spinel and opx that may have larger grain size (Fig. 1c-d). Unlike all other dunites,

367 sample 48-12 is sheared, with irregular fragments of coarse olivine among fine-grained

368 olivine neoblasts (Plate B', ES2). The coarse and shear dunites, unlike olivine megacrysts,

369 have not been previously reported from Udachnaya.

370   (3) Nine "low-opx harzburgites" contain 11–21% opx (Fig. 1g-h) and are similar to coarse

371 dunites in hand specimens in terms of grain size and microstructure. These harzburgites can

372 only be distinguished from coarse dunites using modal and WR major element compositions.

373   (4) Two "opx-rich harzburgites" contain 40–50% opx with grain size larger than for

374 coexisting olivine; they were added to the suite for comparison with the low-opx harzburgites.

375 Late-stage alteration is rare or absent in nearly all the samples, which usually contain non-

376 serpentinized olivine.

377   Modal compositions are given in Table 1 and shown in Fig. 2 as co-variation plots and

378 relative to Mg#$_{WR}$. In general, all the four main xenolith types in this study can be robustly

379 distinguished by modal abundances. The dunites and low-opx harzburgites define a small, but

380 distinctive gap in modal opx: $\geq 11\%$ in the harzburgites vs. $\leq 5\%$ in ten dunites out of eleven

381 (except unusual, metasomatized sample 85-14 with 8.6% opx, Fig. 2a, d). This gap is greater

382 than the uncertainties of modal estimates (*Section 3.1*). Olivine and opx are by far the most

383 abundant minerals, with totals >94%, and define a linear co-variation trend for all the xenolith

384 types, except olivine megacrysts because the latter may contain more garnet (Fig. 2c) than

385 opx (Fig. 2d). Garnet abundances range from 0 to 4–6% and are similar in all the rock groups

386 (averages 2–3%, Table 1).

387

388 4.2. *Major element compositions and P-T estimates*

389   Major element compositions of bulk xenoliths and minerals are given in Table 2 of ES1

390 and shown in Figs. 3-5. The dunites, olivine megacrysts and harzburgites have similar

391 variation ranges of some major elements (Ca, Al, Fe, Cr) as well as of Mg# in bulk samples

392 (Mg#$_{WR}$) (Figs. 3-4) and olivine (Mg#$_{Ol}$). However, the bulk dunites and megacrysts tend to

393 have higher MgO and NiO, but lower SiO_2 and Na_2O (Figs. 3e-f and 4b); they are clearly set

394 apart from the harzburgites by higher Mg/Si$_{mol}$ ratios (≥1.7, Fig. 3b) linked to lower modal

395 opx in the dunites and megacrysts (Fig. 2d). The WR ranges of FeO (6.1–7.9 wt.%) and Mg#

396 (0.917–0.934) are similar for coarse dunites, olivine megacrysts and low-opx harzburgites,

397 and typical of those in refractory cratonic peridotites (Fig. 4a). The bulk variation ranges and

398 average concentrations of CaO (0.13–0.47 wt.%, av. = 0.25 wt.%) and Al_2O_3 (0.02–0.68

399 wt.%, av. = 0.36 wt.%) for megacrystalline dunites are lower than for coarse dunites (0.28–

400 1.04 wt. and 0.56 wt.% CaO; 0.28–1.04 wt.% and 0.56 wt.% Al_2O_3). Sheared dunite 48-12

401 has high FeO (12.5 wt.%) and low Mg# (0.87).

402   The Mg#$_{Ol}$ for coarse peridotites and megacrysts in this study range from 0.920 to 0.934

403 and define a close-fitting linear co-variation with the Mg# of coexisting opx suggesting

404 chemical equilibration, but the plots of Mg#$_{Ol}$ vs. Mg# of garnet and cpx show more scatter

405 (Fig. 5a). The Mg# of garnet (0.79–0.86) is much lower than for coexisting olivine and

406 pyroxenes. The Mg#$_{Ol}$ shows a linear correlation with Mg#$_{WR}$ (Fig. 5c), but xenoliths with

407 high modal abundances of low-Mg# garnet, ilmenite (Mg#$_{Ilm}$ = 0.3) and spinel (Mg#$_{Sp}$ =

408 0.53–0.75) plot off the trend to higher Mg#$_{Ol}$; this is the reason why Mg#$_{Ol}$ alone is not a

409 reliable index of melt extraction for cratonic xenoliths (e.g. Doucet et al., 2013; Ionov et al.,

410   2010).

411   The modal abundances of garnet and pyroxenes are not correlated with Mg#$_{WR}$ (Fig. 2d-f),

412   but the garnet modes are proportional to bulk-rock Al$_2$O$_3$, in particular in dunites (Fig. 5c).

413   The concentrations of Cr$_2$O$_3$ and the Cr#$_{Gar}$ (Cr/(Cr+Al)$_{mol}$ in garnet) define positive

414   correlations with the Cr#$_{WR}$ (Fig. 5d). Together with the Mg#$_{WR}$ vs. Mg#$_{Gar}$ correlation, this

415   suggests that garnet is chemically equilibrated in the peridotites, in spite of local irregularities

416   due to zoning and distinct garnet generations. CaO in garnets shows negative correlations

417   with MgO (close-fitting) and Cr$_2$O$_3$ (dispersed) (Fig. 5c-d).

418   Pressure and temperature (P-T) estimates are problematic in some xenoliths in this study

419   because the most robust thermobarometry methods are based on compositions of coexisting

420   pyroxenes and garnet (e.g. Nimis and Grütter, 2010), whereas not all of these minerals may be

421   present or fully chemically equilibrated due to low abundances and/or the presence of

422   generations with different compositions (Table 2 of ES1). Table 1 gives the list of the thermo-

423   barometers and P-T values calculated for eleven garnet-bearing xenoliths. Temperature

424   estimates for another ten samples that contain pyroxenes, but not garnets are based on fixed P

425   values (3.5 or 4.0 GPa) selected using T projections to a local geotherm (Goncharov et al.,

426   2012), and have much higher uncertainties. The P-T values for the garnet-bearing rocks (783–

427   1154°C; 3.9–6.5 GPa) plot between the model 35 and 40 mW/m^2 conduction geotherms; the

428   T estimates for the other xenoliths fall in the same T range (Fig. 6). Importantly, the dunites

429   show a broad P-T range that overlaps with that earlier reported for coarse garnet peridotites

430   from Udachnaya (Doucet et al., 2013) and thus do not appear to be concentrated within a

431   particular depth range in the lithospheric profile.

432

433   4.3. *Trace element compositions*

434   Trace element compositions (and WR patterns) are given in Tables 4-5 of ES1. The WR

rare earth element (REE) patterns normalized to primitive mantle (PM) show continuous

enrichments in the light (LREE) and medium (MREE) over heavy REE (HREE), but the PM-

normalized abundances decrease for the heaviest REE from Lu to Tm or Ho in many samples

(Fig. 7a, c, d). The WR patterns for lithophile trace elements are more complex, with common

negative Zr-Hf anomalies and positive Nb-Ta anomalies (Fig. 7b, d, f).

The WR enrichments in highly incompatible elements are not likely to be due to direct

contamination by macroscopic veins and pockets of kimberlite, which were avoided during

sample preparation. Besides, the patterns for Udachnaya kimberlites and the xenoliths are

different for some elements like Rb, Ba, Sr (Fig. 7). On the other hand, it appears that a range

of kimberlite-related fluids infiltrated and reacted with the xenoliths shortly before or during

their transport to leave behind melt inclusions and numerous micro-phases (e.g. Golovin et

al., 2019). These may be alkali-carbonate liquids that reacted with host deep mantle to form

primitive kimberlite melts as well as mobile fractionation products of kimberlite magmas.

Garnet is the only accessory mineral analyzed by LA-ICPMS in many xenoliths. Its REE

patterns (Fig. 8) are usually sinusoidal, however garnet 565-10 has an inverted (relative to the

sinusoidal patterns) shape with low MREE (Fig. 8c); such patterns are common for garnets in

coarse Udachnaya peridotites (Agashev et al., 2013; Doucet et al., 2013; Shimizu et al.,

1997). The trace element data suggest that different garnet generations may be present in the

xenoliths. Sample 575-13 contains both the sinusoidal and LREE-depleted (Fig. 8b), but

HREE-MREE-enriched, garnets; the HREE-MREE-enriched patterns are typical for

deformed, mainly melt-metasomatized Udachnaya peridotites (Agashev et al., 2013; Doucet

et al., 2013).

Three WR dunites show positive Eu anomalies (Fig. 7a, c), but the garnets (major HREE-

MREE hosts) in the same samples have no sizeable Eu anomalies. Analyzing small, locally

zoned, garnet grains at low abundances is challenging. The Eu anomalies in the WR xenoliths

460   may be analytical artefacts due to sporadic oxide ($^{135}Ba^{16}O$) interferences with ^{151}Eu (e.g.

461   Ionov et al., 1992). Alternatively, the trace elements in the garnets may not be fully

462   equilibrated with other trace element hosts in the samples, but this is not very likely because

463   major element indices, like Mg# or Cr# (Fig. 5a, d), suggest that the garnets are equilibrated

464   with other minerals. Additional work is required to address the discrepancy.

465

466   4.4. *PGE and Re abundances*

467   The WR abundances of PGE and Re are given in Table 2. The Os concentrations in 23

468   xenoliths range from 0.4 to 15.8 ppb, about half are higher than 3.9 ppb, which is the value

469   inferred for the PM (Palme and O'Neill, 2014) whereas the sheared dunite, one low-opx and

470   two opx-rich harzburgites are very low in Os (0.01–0.04 ppb). Similar Os ranges for coarse

471   Udachnaya peridotites were previously reported by Pearson et al. (1995b) and Ionov et al.

472   (2015b). Average Os concentrations are higher for olivine megacrysts and megacrystalline

473   dunite (8.3 ± 4.5 ppb, 1σ) than for coarse dunites (4.2 ± 2.5 ppb) and low-opx harzburgites

474   (3.7 ± 1.9 ppb), but it is not clear that these differences are meaningful because the Os

475   contents are too varied (high σ), their ranges overlap and the samples are too few. The broad

476   Os variations in the xenoliths in this study are not likely to be due to the "nugget effect"

477   (sampling or analytical) alone, but may reflect heterogeneous Os distribution in the mantle on

478   a large scale, possibly due to metasomatism-related PGE mobility (e.g. Reisberg et al., 2005).

479   Re concentrations in all but four samples are at or below the PM value (0.35 ppb).

480   PM-normalized (Becker et al., 2006) patterns for PGE and Re are shown in Fig. 9. The

481   levels and patterns for Os, Ir and Ru are similar for the majority of dunites, megacrysts and

482   harzburgites, except four low-Os rocks and two other samples that have unusually high or low

483   Os/Ir ratios. Five megacrystalline xenoliths (Fig. 9a) show continuous depletions in Pt, Pd and

484   Re relative to Os, Ir, and Ru. Six coarse dunites show similar trends whereas another three

485   coarse dunites show Re-enrichments and irregular PGE patterns (Fig. 9b). The harzburgites

486   show the greatest range of patterns. All of them are depleted in Pt and Pd relative to Os-Ir-Ru,

487   but some are depleted in Pt relative to Pd and/or enriched in Re relative to Pd (Fig. 9c).

488

489   4.5. *Re-Os isotope systematics*

490   The $^{187}Re/^{188}Os$ and $^{187}Os/^{188}Os$ ratios are given in Table 2, together with $^{187}Os/^{188}Os$

491   values recalculated to the eruption age of the host kimberlite (~360 Ma) using the ^{187}Re decay

492   constant ($\lambda^{187}Re$) of $1.666 \pm 0.005 \times 10^{-11}$ a^{-1} (Smoliar et al., 1996), and model T_{RD} and T_{MA}

493   ages calculated with PM (PUM) estimates for $^{187}Os/^{188}Os = 0.1296$ (Meisel et al., 2001) and

494    $^{187}Re/^{188}Os = 0.4353$ (Becker et al., 2006); the $^{187}Os/^{188}Os$ values at the eruption age were

495   used to obtain the T_{RD} values.

496   The samples in this study define a positive $^{187}Os/^{188}Os$ vs. $^{187}Re/^{188}Os$ (Fig. 10a) linear

497   correlation ($^{187}Os/^{188}Os = 0.0062 \times^{187}Re/^{188}Os + 0.1129$) with a slope equivalent to an age of

498   0.37 Ga, which is identical to the eruption age of host kimberlite (see *Section 2.1*). The slope

499   (hence the age) is mainly defined by a subset of ten xenoliths with very high $^{187}Re/^{188}Os$ and

500   appears to be robust, e.g. it is little affected if any of the samples with the highest $^{187}Re/^{188}Os$

501   and $^{187}Os/^{188}Os$ are removed one after another. Six of these samples are very low in Os (<0.7

502   ppb; ≤0.04 ppb in 4 samples); high $^{187}Re/^{188}Os$ (0.7–4.8) in the other four xenoliths are due to

503   a combination of high Re (0.3–0.7 ppb) and low to moderate Os. It appears that Re

504   enrichments and Os depletions are linked to processes that were coeval with, or operated

505   shortly before, the kimberlite eruption. Both T_{RD} and T_{MA} estimates for these xenoliths appear

506   to have high uncertainty and may not be well-suited to constrain their melt-extraction age; the

507   T_{MA} for these samples are very low and usually negative (Table 2).

508   Sixteen xenoliths that show no apparent Os-depletions ([Os] ≥1.8 ppb) and Re-enrichments

509   are most fitting to constrain melt extraction ages. The $^{187}Os/^{188}Os$ ratios in dunites and olivine

510   megacrysts among those samples (0.1066–0.1125) are lower than in harzburgites (0.1145–

511   0.1157) while their $^{187}Re/^{188}Os$ ranges are similar (Fig. 10b). As a result, the T_{RD} ages for the

512   dunites and megacrysts (2.4–3.1 Ga; average 2.8 Ga) are higher than for the harzburgites

513   (1.9–2.1 Ga; average 2.0 Ga). Five megacrystalline xenoliths define a positive $^{187}Os/^{188}Os$ vs.

514     $^{187}Re/^{188}Os$ linear correlation (Fig. 10b) with an 'isochron' age of 2.7 ± 1.2 Ga and an initial

515     $^{187}Os/^{188}Os$ of 0.1069 ± 0.0017. The fields of dunites plus megacrysts on plots of T_{RD} ages vs.

516   modal olivine and opx are distinct from the fields for the harzburgites (Fig. 11).

517

518   **5. Discussion**

519   5.1. *The record of melt extraction and metasomatism in the Udachnaya peridotites*

520   Coarse cratonic peridotites typically have high $Mg\#_{WR} \geq 0.92$ and low Al and Ca (e.g.

521   Carlson et al., 2005), and are believed to be residues of 35–45% melting of fertile mantle at

522   about 3 to 7 GPa based on experimental studies (e.g. Walter, 1999). Spinel harzburgites from

523   Udachnaya were earlier interpreted as nearly pristine, in terms of modal and major oxide

524   compositions, residues of 35–38% polybaric melt extraction (Doucet et al., 2012; Ionov et al.,

525   2010), but garnet peridotites from Udachnaya commonly show evidence for modal

526   metasomatism after melt extraction (Agashev et al., 2013; Doucet et al., 2013).

527   The content of Al_2O_3, CaO and FeO in some dunites and low-opx harzburgites in this study

528   is about the same or even lower than in the spinel harzburgites from the earlier work (Fig. 4a)

529   suggesting that they experienced similar, or even higher, degrees of melt extraction. Other

530   xenoliths, however, contain more Al_2O_3 than relevant experimental melt extraction residues

531   (Fig. 4b). The content of Al_2O_3 in our samples is not related to $Mg\#_{WR}$ (Fig. 3a), which is

532   hard to explain in terms of Al variation due to different melting degrees, but is proportional to

533   modal garnet (Fig. 5c). Small amounts of garnet in refractory cratonic peridotites may form

534   by exsolution from opx on cooling after melting (Doucet et al., 2013), but dunites and olivine

535   megacrysts in this study contain little, if any, opx. Thus, it appears that some samples in this

536   study experienced moderate post-melting enrichments in Al, likely linked to garnet formation,

537   even though the content of Al_2O_3 is often considered to be a robust melt extraction index for

538   residual peridotites (e.g. Reisberg and Lorand, 1995; Rudnick and Walker, 2009).

539   Clinopyroxene and ilmenite were formed by metasomatism as well; the cpx-bearing

540   samples show enrichments in Ca (Fig. 3d) and usually have CaO $\geq Al_2O_3$ (Table 1) while the

541   ilmenite-bearing xenoliths have $TiO_2 \geq 0.06$ wt. %.

542   Very low HREE contents in the dunites, megacrysts and low-opx harzburgites (0.01–0.1 $\times$

543   PM; Fig. 7) and PM-normalized values that decrease from Lu up to Ho (i.e. in the direction of

544   lower compatibility) also suggest that the protoliths for these xenoliths formed by high-degree

545   melt extraction. However, trace element data, e.g. WR patterns with remarkably regular

546   enrichments from HREE to MREE and LREE, suggest that all the xenoliths were

547   subsequently affected by post-melting metasomatism, in line with the common presence of

548   metasomatic garnet, cpx and ilmenite. The LREE are positively correlated with CaO and may

549   be mainly hosted in Ca-rich accessory phases. Megacrystalline xenoliths show the largest

550   REE range, but coarse dunites have higher average LREE-MREE as a group (Fig. 7). MREE-

551   LREE enrichments were reported for olivine separated from Udachnaya megacrysts (Pernet-

552   Fisher et al., 2019) as well, but at concentrations an order of magnitude lower.

553   A dunite and a harzburgite, in which ilmenite was found in thin sections and/or crushed

554   rocks, have the highest positive Nb-Ta anomalies (Fig. 7), suggesting that the Nb-Ta

555   enrichments in several other xenoliths in this study may be due to accessory metasomatic

556   ilmenite as well. Occasional Sr enrichments may suggest the presence of mantle-derived

557   carbonates (e.g. Ionov, 1998), like those in xenoliths from Obnazhennaya (Ionov et al.,

558   2018b), but no carbonates were found in thin sections.

559   The origin of dunites and megacrystalline olivine in cratonic mantle remains controversial.

560   Dunite formation has been attributed to high-degree melting either in nominally anhydrous

561   upwelling mantle (ancient plumes or spreading environments) (e.g. Herzberg, 2004; Servali

562   and Korenaga, 2018), or in subduction zones and their Archean equivalents supposing that the

563   presence of water may enhance melting (Liu et al., 2018; Pearson and Wittig, 2008; Wittig et

564   al., 2008). Bernstein et al. (2006) reported dunite and low-opx harzburgite xenoliths from

565   West Greenland (too small to obtain WR samples) with the ranges of $Mg\#_{Ol}$ (0.920–0.937)

566   and $Cr\#_{Spl}$ (0.47–0.96) similar to those in this study, and suggested that these rocks formed by

567   dry melting to the point of opx exhaustion in the Archean. By contrast, Pearson and Wittig

568   (2008) argued for the presence of water during melting to form dunites from another West

569   Greenland site and speculated that migration of siliceous melts produced by opx breakdown

570   may produce opx-rich harzburgites, like those in this study and earlier work on Udachnaya

571   (Boyd et al., 1997; Doucet et al., 2012; Ionov et al., 2010). Alternatively, dunite formation in

572   mantle lithosphere was attributed to reaction of harzburgites with migrating mafic melts that

573   breaks down and removes opx (e.g. Kelemen et al., 1990). The origin of megacrystalline

574   olivine remains a mystery.

575   The Re-Os dating of xenoliths in this study provides an important argument in this debate

576   by establishing that Udachnaya dunites and olivine megacrysts are systematically older than

577   low-opx harzburgites. For instance, the Udachnaya dunites cannot be melt channel materials

578   (Kelemen et al., 1990), by contrast to dunites hosted by the Obnazhennaya kimberlite in the

579   NE Siberian craton that have younger T_{RD} ages and lower Mg# than harzburgites (Ionov et

580   al., 2015a). Similarly, the Udachnaya dunites and olivine megacrysts cannot have been

581   produced by re-melting in subduction zones of older harzburgites formed in ocean ridge

582   settings (Pearson and Wittig, 2008). Finally, the change in modal compositions from Archean

583   dunites to Proterozoic harzburgites cannot be attributed to cooling of the mantle after the late

584 Archean (Herzberg et al., 2010) because they have similar Mg#, Al and Ca ranges, but

585 distinct Mg/Si ratios (Fig. 3), and because harzburgites in other cratons usually have Archean

586 ages.

587

588 5.2. *The distribution of PGE and Re in the mantle beneath Udachnaya*

589   This study provides the first HSE data for coarse WR dunites and an orthopyroxenite from

590 Udachnaya as well as for bulk large olivine megacrysts rather than their fragments or pure

591 olivine. The abundances and patterns of HSE in 17 WR coarse harzburgites (as well as in

592 lherzolites and deformed peridotites) from Udachnaya were reported by Ionov et al. (2015b);

593 they are generally similar to those in this study. Literature data for olivine separated from

594 small Udachnaya peridotite xenoliths often show very low Os concentrations (Pearson et al.,

595 1995b; Pernet-Fisher et al., 2015) apparently because pure olivine is very low in Os (e.g.

596 Burton et al., 2000) and because Os hosts (alloy and sulfide micro-phases) may be unevenly

597 distributed (e.g. Aulbach et al., 2016). By comparison, reported Os concentrations in

598 fragments of eight high-Mg# olivine megacrysts from Udachnaya (Pearson et al., 1995b;

599 Pernet-Fisher et al., 2019) are consistently high (0.4–10.7 ppb; av. = 4.4 ± 4.0 ppb (1σ)) and

600 overlap those for coarse dunites and bulk megacrysts from this study (Plate 6, ES1). We posit

601 that Os in coarse peridotites including dunites reside mainly in intergranular micro-phases,

602 while Os in megacrystalline olivine-rich xenoliths may be hosted by inclusions in olivine.

603   Experimental evidence and studies of natural samples have shown that Os and Ir are

604 compatible during partial melting of fertile mantle and that as melting proceeds move from

605 sulfides into Os-Ir alloys in refractory residues (e.g., Brenan and Andrews, 2001). By

606 contrast, Pt and Pd are compatible to slightly incompatible at low to moderate melting

607 degrees, but are largely extracted from the residues after 20–25% of melting when sulfides are

608 exhausted (e.g. Pearson et al., 2004). The HSE concentrations and patterns in megacrystalline

609 xenoliths and the majority of coarse dunites and low-opx harzburgites in this study (Fig. 9)

610 are consistent with well-known HSE behavior during melt extraction. The Os, Ir and Ru

611 concentrations in these samples are close to or somewhat higher than in PM as expected from

612 mass-balance calculations for compatible elements in melting residues and commonly

613 observed in cratonic peridotites (Aulbach et al., 2016; Ionov et al., 2015b; Pearson et al.,

614 2004). By contrast, PM-normalized Pt, Pd and Re abundances in the majority of the samples

615 decrease steadily due to incompatible behavior at high melting degrees.

616   Seven coarse dunites and harzburgites (including two high-opx harzburgites) show

617 complex HSE patterns in Fig. 9. All of them have high Re/Os ratios, six are enriched in Re

618 over Pt-Pd and four are very low in Os. As shown in *Section 4.5* and Fig. 10a, these samples

619 define a positive linear $^{187}Re/^{188}Os$ vs. $^{187}Os/^{188}Os$ correlation corresponding to the eruption

620 age of host kimberlite, and close to those obtained by Pearson et al. (1995b) and Ionov et al.

621 (2015b) for Udachnaya peridotites with high Re/Os ratios. We see this as evidence that both

622 the Re enrichments and PGE mobility are caused by some kind of interaction of the rocks

623 with kimberlite-related media, most likely shortly before the transport of the xenoliths by

624 kimberlite eruption, as shown earlier for sheared Udachnaya peridotites (Golovin et al., 2018;

625 Golovin et al., 2019). By contrast, we see no robust evidence in hand specimens, thin sections

626 or chemical analyses for intrusion of the WR samples by bulk kimberlite material during the

627 eruption. For instance, Re concentrations in the kimberlites (0.11–0.16 ppb) (Ionov et al.,

628 2015b) are too low to account for Re enrichments in the xenoliths; some trace element ratios

629 in the kimberlites are different from those in the xenoliths (Fig. 7; see *Section 4.3*).

630   The fact that no low-Os, high-Re samples are found among megacrystalline xenoliths

631 may be related to their unusually large grain size, hence low permeability. Two opx-rich

632 harzburgites analyzed are very low in Os, but they are too few to infer that this is typical for

633 this rock type. Ionov et al. (2015b) found seven low-Os xenoliths among 29 Udachnaya

634 peridotites analyzed; all of them were garnet- and cpx-bearing harzburgites affected by modal

635 metasomatism. They speculated that at some conditions (high T, specific melt compositions,

636 oxygen fugacity) metasomatism may mobilize and remove Os and other PGE from refractory

637 residues (e.g. Aulbach et al., 2016; Wittig et al., 2010a). Because all the low-Os coarse

638 Udachnaya peridotites are Mg-rich (Mg# 0.922–0.934), the hypothetical percolating melts

639 must have high Mg# and/or be low in iron (e.g. Na-Ca-Mg carbonatites). On the other hand,

640 PGE+Re patterns in many strongly metasomatized xenoliths in this study (e.g. ilmenite-

641 bearing and those with the highest modal garnet, cpx and LREE) are not perturbed.

642   The origin of sheared dunite 48-12 that has both low PGE abundances and low Mg# is

643 uncertain. Its lithophile trace element pattern is very similar to that of olivine megacryst U220

644 (Plate 4a, ES1). Sheared Udachnaya peridotites reported by Ionov et al. (2015b) have higher

645 PGE concentrations, and some have nearly flat, PM-like PGE+Re patterns. These rocks have

646 high Pt-Pd and Re abundances in spite of (or due to?) melt-metasomatism (e.g. Luguet et al.,

647 2015) that accompanied shearing in these rocks. Olivine orthopyroxenite 194-13, which most

648 likely is of magmatic origin, has a convex-up PGE+Re pattern with maxima for Ru and Pt.

649

650 5.3. *Constraints on the use of Re-Os isotope data for melt-depletion age estimates*

651   Constraining the age of the xenoliths involves several types of uncertainties. One of them

652 relates to ubiquitous post-melting Re-enrichments, which are commonly linked to processes

653 coeval with the eruption of host magma. This is a problem common to Re-Os studies of

654 xenoliths that led to the definition of the Re-depletion model age (T_{RD}: Walker et al. (1989)).

655 T_{RD} ages are calculated by first correcting the $^{187}Os/^{188}Os$ ratios measured in each sample

656 back to the age of the host volcanic rock using each sample's Re/Os ratio to account for any

657 Re-addition that presumably occurred at the time of the eruption. The calculated initial

658 $^{187}Os/^{188}Os$ is then compared with the Os isotope evolution of pristine undifferentiated mantle

659   assuming that the sample had a Re/Os ratio of zero prior to its capture by the host magma. If

660   the sample had a non-zero Re/Os ratio while still in the mantle, the T_{RD} approach provides

661   only a minimum estimate to the time of Re-depletion through melt extraction.

662   This approach works well for xenoliths with relatively low Re/Os ratios, but its ambiguity

663   increases with increasing Re/Os ratios measured in a sample, and also depends on (a) the

664   exact knowledge of the eruption age and (b) the absence of pre-eruption Re enrichments.

665   Nearly all the samples in this study are highly refractory melt extraction residues (*Section*

666   *5.1*), and it is reasonable to assume that they had negligible Re abundances after their

667   formation and thus are likely to yield robust melt extraction age estimates. Very high

668   $^{187}Re/^{188}Os$ (up to 4.8) of several xenoliths in this study result in large, and hence uncertain,

669   eruption age corrections for $^{187}Os/^{188}Os$ and T_{RD} values. We evaluated uncertainties related to

670   the eruption age of the host kimberlite (~360 Ma) by recalculating initial $^{187}Os/^{188}Os$ ratios

671   with eruption ages of 390 Ma and 330 Ma for the xenoliths with high Re/Os ratios and

672   obtained significant T_{RD} variations ranging from ±0.06 Ga for sample 615-09 to ±0.3 Ga for

673   sample 63-13. Re enrichments by ancient metasomatism may affect T_{RD} estimates even more.

674   To minimize such uncertainties, we disregard T_{RD} estimates for samples with $^{187}Re/^{188}Os$

675   ratios higher than the PM value (0.435; Becker et al. (2006)) as well as for dunite 85-14

676   because its $^{187}Os/^{188}Os$ ratio is too radiogenic for an ancient melt extraction residue and more

677   consistent with Re enrichments long before the kimberlite eruption. Altogether, we examine

678   below the age estimates for five low-opx harzburgites and eleven dunites and megacrysts,

679   $^{187}Re/^{188}Os$ in these samples ranges from 0.02 to 0.13 (Table 2).

680   Uncertainties in Re-Os model ages are also related to the choice of different models for the

681   hypothetical undifferentiated upper mantle reservoir (Bulk Silicate Earth, BSE) that was

682   melted to yield residual mantle peridotites. The T_{RD} and T_{MA} ages in this study are calculated

683   with the commonly used primitive upper mantle (PUM or PM) model based on fertile mantle

684   peridotites: ^{187}Os/^{188}Os = 0.1296 ± 0.0008 (Meisel et al., 2001) and ^{187}Re/^{188}Os = 0.435 ±

685   0.010 (Becker et al., 2006). An earlier version of this model reported a slightly lower

686   ^{187}Os/^{188}Os of 0.1290 (Meisel et al., 1996).

687   Alternative BSE models are based on the compositions of different groups of chondrites.

688   Shirey and Walker (1998) reported present-day chondritic reference values of ^{187}Os/^{188}Os$_{ch}$ =

689   0.127 and ^{187}Re/^{188}Os$_{ch}$ = 0.40186. Walker et al. (2002a) showed that carbonaceous

690   chondrites have a distinctively low average ^{187}Os/^{188}Os (0.1262 ± 0.0006; ^{187}Re/^{188}Os = 0.392

691   ± 0.015) while enstatite (^{187}Re/^{188}Os = 0.421 ± 0.013; ^{187}Os/^{188}Os = 0.1281 ± 0.0004) and

692   ordinary (^{187}Re/^{188}Os = 0.422 ± 0.025; ^{187}Os/^{188}Os = 0.1283 ± 0.0017) chondrites overlap with

693   a mean of 0.1282. The latter value is within error of the Os isotopic composition of

694   convecting upper mantle deduced from ophiolite chromites (^{187}Os/^{188}Os = 0.1281 ± 0.0009;

695   (Walker et al., 2002b)). If the PUM composition was set via addition of a late veneer of

696   planetesimals, it appears that the veneer was dominated by ordinary and enstatite chondrites.

697   Incorrect use of the model parameters may lead to erroneous T_{RD} and T_{MA} values and

698   considerable confusion in comparison of mantle formation ages, e.g. as shown recently for

699   xenoliths from Obnazhennaya in the NE Siberian craton (Ionov et al., 2018a). The differences

700   in T_{RD} ages based on contrasting BSE models for ≥3 Ga old cratonic peridotites may be as

701   high as 0.3 Ga (e.g. Carlson et al., 1999). BSE reference values in some previous Re-Os work

702   on Udachnaya xenoliths are different from those in this study. Pearson et al. (1995b) used

703   ^{187}Re decay constant = 1.64×10^{-11} a^{-1}, ^{187}Re/^{188}Os = 0.397 and ^{187}Os/^{188}Os = 0.12757. Pernet-

704   Fisher et al. (2015) and Pernet-Fisher et al. (2019) used the chondrite average from Shirey and

705   Walker (1998) for ^{187}Os/^{188}Os = 0.127, but a ^{187}Re/^{188}Os = 0.3935 (CV3 chondrite Allende ?).

706   The model ages from these papers were recalculated using the PUM model (Plate 6 of ES1)

707   for comparison with data in this study. In addition, Table 2 shows T_{RD} and T_{MA} for samples in

708   this study calculated with the chondritic model of Shirey and Walker (1998); the differences

709   in model ages using the two BSE models are ≤0.2 Ga for nearly all the samples (ES1).

710

711   5.4. *Formation age of refractory lithospheric mantle in the central Siberian craton*

712   T_{RD} ages for low-opx harzburgites (1.9–2.1 Ga; average 2.0 ± 0.1 Ga (1 σ)) are manifestly

713   younger than for dunites and olivine megacrysts (2.4–3.1 Ga; av. 2.8 ± 0.2 Ga) among the 16

714   low-Re/Os xenoliths in this study deemed most fitting for T_{RD} age estimates. All these

715   samples also yield coherent T_{MA} values, which are slightly older than the T_{RD} ages, with T_{MA}

716   averages of 2.2 ± 0.3 Ga for the harzburgites and 3.2 ± 0.2 Ga for the dunites and olivine

717   megacrysts. By contrast, T_{MA} for the high-Re/Os samples are very low and usually negative

718   (Table 2). As discussed in the previous section, we consider that T_{RD} estimates for such

719   samples cannot be viewed as robust melt extraction ages because the effects of Re addition by

720   post-melting processes are too large to be accurately corrected. The T_{RD} range for all nine

721   low-opx harzburgites in this study (including four high-Re/Os samples) is much wider (1.5–

722   2.4 Ga), but the average (2.0 ± 0.3 Ga) is not very different from that obtained for samples

723   with low Re/Os alone. Overall, the screening procedure to discard samples with perturbed

724   Re/Os ratios allows to better constrain the T_{RD} range for the harzburgites by reducing the data

725   scatter, and thus to clearly discern it from the T_{RD} range for the dunites and megacrysts (Figs.

726   10-12).

727   Previous work on Re-Os dating of Udachnaya peridotite xenoliths reported a much greater

728   proportion of samples with high Re/Os ratios than in this study, hence potentially more T_{RD}

729   scatter. $^{187}Re/^{188}Os$ in eight coarse peridotites reported by Pearson et al. (1995b) range from

730   0.23 to 27; four of these samples have $^{187}Re/^{188}Os$ ≤1.5 and yield Paleoproterozoic T_{RD} (2.0–

731   2.2 Ga; av. 2.1 ± 0.1) calculated with the PUM model as in this study (Table 6 of ES1). Ionov

732   et al. (2015b) reported nine coarse harzburgites with $^{187}Re/^{188}Os$ from 0.13 to 2.5 and T_{RD}

733   from 1.4 to 2.2 Ga, and chose six of them as best representing melt extraction ages (2.0–2.2

734   Ga; av. 2.1 ± 0.1 Ga). The data from previous studies overlap the T_{RD} range for low-opx

735   harzburgites in this study (1.9–2.1 Ga; av. 2.0 ± 0.1 Ga) obtained on samples with $^{187}Re/^{188}Os$

736   ≤0.126, which we consider the best current age estimate for this rock type (Fig. 12a). Overall,

737   the Paleoproterozoic formation at ~2 Ga for coarse harzburgites, which make up the greatest

738   portion of the refractory protolith of lithospheric mantle beneath Udachnaya, is now firmly

739   established by several studies and cannot be ignored when discussing the age and history of

740   the Siberian craton.

741   This study is the first to identify and characterize coarse (≤5–10mm) dunites, as defined in

742   *Section 4.1*, i.e. distinct from previously reported olivine megacrysts and "megacrystalline

743   dunites", among Udachnaya xenoliths. The coarse dunites are hard to tell from low-opx

744   harzburgites in hand specimens and were identified here using modal and major oxide

745   abundances. Coarse dunites are nearly impossible to recognize in the field, and can be easily

746   overlooked. By contrast, megacrystalline xenoliths can be set apart in hand specimens and in

747   the field based on olivine ≥1 cm. The T_{RD} ranges and averages for olivine megacrysts (2.4–

748   3.0 Ga, av. 2.6 ± 0.2 Ga) and coarse dunites (2.5–3.1 Ga, av. 2.9 ± 0.2 Ga) in this study are

749   not very different (within ~1σ for averages) (Fig. 12a). If these two xenolith types have

750   different origins and formed in distinct events, their formation may be roughly coeval.

751   The meaning of the 'isochron' defined by the megacrystalline xenoliths in Fig. 10b is not

752   clear. One option could be to ascribe the isochron to an event ~2.7 Ga ago that produced a

753   range of Re/Os ratios in parts of a protolith with an initial $^{187}Os/^{188}Os$ of 0.1069 that have

754   since developed the $^{187}Os/^{188}Os$ values measured in these samples. In such a case, the

755   formation age of the megacrystalline suite in this study could be ~2.7 Ga, not much different

756   from its average T_{RD} of 2.6 ± 0.2 Ga (Table 2). However, this isochron age is too uncertain

757   because of high error (±1.2 Ga) to warrant such an inference.

758   Alternatively, based on model ages in the combined dunite and megacryst population (Fig.

759 12a), they can be grouped in two subsets with much more tightly clustered ages: six samples

760 with the T_{RD} range of 2.4–2.7 Ga (av. 2.6 ± 0.1 Ga) and five with the T_{RD} range of 2.8–3.1 Ga

761 (av. 3.0 ± 0.1 Ga). Average T_{MA} estimates for the same xenoliths are 3.0 ± 0.2 Ga and 3.3 ±

762 0.1 Ga. The average T_{RD} ages in these two clusters are distinct within ±2σ, which may imply

763 that they formed in two distinct Archean events. In such a case, the difference in grain size

764 between the megacrysts and coarse dunites may not be related to age, and possibly unrelated

765 to the formation mode of their protoliths.

766 Pearson et al. (1995b) reported Re-Os data on five "megacrystalline peridotites" that have

767 0.6–2.6 ppb Os, $^{187}Re/^{188}Os$ of 0.12–0.97 and T_{RD} of 1.9–2.8 Ga (re-calculated with the PUM

768 model, Table 6 of ES1). The T_{RD} in these samples fall in two groups: ~1.9 Ga and 2.8–3.2 Ga;

769 the latter range is only slightly higher than for dunites and megacrysts in this study (Fig. 12a).

770 These results are hard to compare directly with our dataset because they were obtained not on

771 representative WR samples, like in this study, but on small amounts of material extracted

772 from xenoliths, for which no other data were reported, except that their $Mg\#_{Ol}$ range

773 overlapped that for coarse peridotites from the same suite.

774 Pernet-Fisher et al. (2019) obtained Archean T_{RD} values (2.5–3.1 Ga, av. = 2.9 ± 0.2 Ga;

775 re-calculated with the PUM model, Plate 6 of ES1) for pure olivine separated from seven

776 megacrysts with Mg# >0.92 from Udachnaya, and aberrant T_{RD} for megacrysts with lower

777 Mg#. The T_{RD} ranges and averages for the Mg-rich olivine are similar to those for megacrysts

778 (as well as dunites) in this study (Fig. 12a). By contrast, olivine separated from many

779 peridotite xenoliths from Udachnaya and Obnazhennaya (Pernet-Fisher et al., 2015) showed

780 low Os, high Re/Os and invalid Re-Os model ages contrary to the commonly held view that

781 olivine provides a good measure of whole rock Re-Os systematics in peridotites (see also

782 Ionov et al., 2015a). The olivine separates from Udachnaya megacrystalline xenoliths have

783 consistently high Os concentrations as well (*Section 5.2*), which may suggest that Os in these

784   megacrysts is hosted by micro-inclusions in olivine, which may make them adequate for T_{RD}

785   estimates, unlike for peridotite xenoliths where much Os may be hosted by intergranular

786   materials.

787

788   5.5. *Multi-stage formation of the Siberian craton*

789   This study firmly establishes that various dunites are the oldest peridotites in the mantle

790   beneath Udachnaya, in addition to earlier work that reported Archean (as well as younger)

791   T_{RD} ages for olivine megacrysts and samples designated as "megacrystalline dunites" with

792   unknown modal and bulk chemical compositions (Pearson et al., 1995b; Pernet-Fisher et al.,

793   2019). To evaluate the role of dunites and megacrystalline olivine in the origin and evolution

794   of the lithospheric mantle it is important to constrain their abundance and position in the

795   lithosphere. The dunites and megacrysts in this study come from a broad depth range (≤120–

796   210 km; Fig. 6) and are not restricted to a particular lithospheric layer. Russian sources cited

797   by Boyd et al. (1997) estimated the proportion of "megacrystalline peridotites" at ~3% of

798   Udachnaya xenolith population without specifying how the value was obtained. This estimate

799   appears to be exaggerated. Shiny, coarse olivine crystals draw more attention than other

800   xenolith materials and may seem more common. Our field data suggest that dunites and

801   olivine crystals >2–3 cm in size are very rare in Udachnaya-East kimberlites and much

802   smaller than xenoliths of other peridotites and eclogites, consistent with the absence of bulk

803   analyses of "megacrystalline dunites" in the literature. Their mass proportion among mantle

804   xenoliths may be very low.

805   Boyd et al. (1997) speculated that very coarse peridotites are rare among Udachnaya

806   xenoliths because they disintegrate during eruption faster than fine-grained rocks. We see no

807   reason to suppose that "megacrystalline dunites" are less solid than rocks with smaller grain

808   size or less olivine; the opposite may be true. Fine-grained, sheared peridotites may be

809   abundant among Udachnaya xenoliths not because they are more solid, but because they form

810   in the vicinity of magma feeders due to interaction with proto-kimberlite melts, hence are

811   more likely to be captured by the magma when eruption starts (e.g. Doucet et al., 2014).

812   Because harzburgites are by far the most common type of coarse peridotites among

813   Udachnaya xenoliths, the main part of the existing mantle lithosphere beneath Udachnaya

814   formed in the Paleoproterozoic, as previously suggested by Ionov et al. (2015b). This study

815   offers more precise age estimates for this event constrained by the T_{RD} range for low-opx

816   harzburgites (Table 2): 1.9–2.1 Ga (average 2.0 ± 0.1 Ga) based on the PUM model, and 1.8–

817   2.0 Ga (average 1.9 ± 0.1 Ga) based on the chondrite model of Shirey and Walker (1998).

818   Further support for the Paleoproterozoic formation age comes from Lu-Hf model and

819   isochron ages (1.7–1.9 Ga) reported by Doucet et al. (2015) for cpx-bearing spinel

820   harzburgites as well as Re-Os dating of sulfide inclusions in diamonds from Udachnaya,

821   which yield 1.8 Ga isochron ages (Wiggers de Vries et al., 2013).

822   This study further indicates that, given the predominance of Paleoproterozoic ages for the

823   most typical lithospheric peridotites from Udachnaya, the rare older components may be relict

824   materials, i.e. fragments of ancient lithospheric mantle formed in the Archean that were

825   incorporated into cratonic roots during the final assembly of the central Siberian craton in the

826   Paleoproterozoic (Ionov et al., 2015b; Moyen et al., 2017). Our data give new insights into

827   the earliest lithospheric formation stages in the central Siberian craton.

828   Our preferred interpretation of the Re-Os model ages for the dunites and megacrysts in

829   this study is that they record two distinct Archean events, one in the Neoarchean and the other

830   one in the early Mesoarchean. The lower age limits for these two events are constrained by

831   the T_{RD} values (2.6 ± 0.1 Ga and 3.0 ± 0.1 Ga) and the upper age limits by the T_{MA} values (3.0

832   ± 0.2 Ga and 3.3 ± 0.1 Ga). The mean T_{RD} ages of ~2.6 and ~3.0 Ga (Fig. 12a) may be closer

833   to true values considering that Re in these highly refractory samples must be dominated by

834   post-melting additions. Model ages calculated using the BSE model of Walker et al. (2002a),

835   based on ordinary and enstatite chondrites, are only slightly lower with the T_{RD} of 2.5 ± 0.1

836   Ga and 2.9 ± 0.1 Ga and the T_{MA} of 2.9 ± 0.1 Ga and 3.2 ± 0.1 Ga. These two age groups

837   comprise both coarse dunites and megacrystalline xenoliths suggesting no links between

838   olivine grain size and age, contrary to speculations in earlier work (Pearson et al., 1995b).

839   Sobolev et al. (1984) and Pokhilenko et al. (1993) asserted that many megacrystalline

840   dinites contain diamonds (none has been found in samples from this study). Because diamond

841   formation in peridotites is commonly linked to metasomatism, the large olivine grain size in

842   this rock type could be linked to reworking and recrystallization of coarse dunites. Re-Os ages

843   of sulfide inclusions in Udachnaya diamonds (Wiggers de Vries et al., 2013) indicate that this

844   may have happened ~0.2 Ga after the major stage of lithospheric formation at 2.0 Ga, which

845   appears to be a reasonable time for thickening and cooling of initial melting residues to allow

846   for diamond formation at depths ≥130 km (Fig. 6).

847   A prolonged, multi-stage formation of the Siberian lithospheric mantle is consistent with

848   recent data on crustal basement ages. U-Pb zircon ages for crustal xenoliths from Udachnaya

849   (Moyen et al., 2017) show that lower crustal granulites formed in the Proterozoic (1.83–1.87

850   Ga) whereas tonalities and other upper crustal rocks formed in the Archean (2.71–2.73 Ga).

851   They inferred that the deep lithosphere beneath Udachnaya did not form in a single Archaean

852   event, but grew in at least two distinct events, first in the late Archaean, then in the

853   Paleoproterozoic when a large-scale delamination and rejuvenation of the Archaean lower

854   crust and lithospheric mantle took place. The crustal xenoliths show no evidence for

855   Mesoproterozoic crustal formation (Fig. 12b), and thus do not support mantle melting at ~1.2

856   Ga evoked by Pernet-Fisher et al. (2015).

857   The crustal basement in the central Siberian craton is hidden under a thick sedimentary

858   cover, but is exposed on the Anabar shield in the north (KML file), which appears to belong

859   to the same tectonic unit (Daldyn block) as Udachnaya (Rosen, 2002). Zircons in modern

860   sediments from the Anabar shield (Paquette et al., 2017) define three U-Pb age ranges: 3.0–

861   3.4 Ga, 2.4–2.8 Ga and 1.8–2.0 Ga, with the youngest event linked to the amalgamation of the

862   craton by welding of Archean domains. Similar U-Pb ages were obtained for detrital zircons

863   from Meso- and Neoproterozoic sedimentary basins at the western (2.6–2.5 and 1.9–1.85 Ga)

864   and NE (2.9–2.7 and 2.1–1.95 Ga) margins of the craton (Priyatkina et al., 2016).

865   To sum up, the U-Pb zircon ages from the crustal basement outline three main stages of

866   crustal growth in the northern and NE Siberian craton: 3.0–3.4 Ga, 2.4–2.8 Ga and 1.8–2.0

867   Ga, with the number of zircons increasing from the older to younger ages (Fig. 12b). These

868   stages overlap the three intervals of lithospheric mantle formation (melt extraction) for

869   refractory peridotites in this study (Fig. 12a,b). This conclusion is robust relative to the

870   uncertainties related to Re-Os dating of mantle peridotites, i.e. T_{RD} versus T_{MA} ages and the

871   PUM vs. chondritic BSE composition models. Overall, similarities of U-Pb ages of zircons

872   from the crustal basement and formation ages of refractory peridotites in this study suggest

873   temporal coupling, and possibly genetic links, between crust and mantle formation in the

874   building of the cratonic lithosphere beneath the central Siberian craton (Moyen et al., 2017).

875   An intriguing question, to which we may not have an answer as yet, is if the Udachnaya

876   dunites have preserved the modal and chemical composition of the original Archean mantle

877   lithosphere, or alternatively, were extensively modified during its disruption and reworking in

878   the Paleoproterozoic. The distribution and composition of peridotite xenoliths with Archean

879   ages at Udachnaya are different from those in the Obnazhennaya kimberlite at the NE margin

880   of Siberian craton where Paleoproterozoic and Archean peridotites occur in similar

881   proportions and have similar compositions (Ionov et al., 2015a). On the other hand, the

882   lithospheric mantle compositions and ages may differ in different parts of the Siberian craton.

883   Another unresolved question is how the minor domains of Archaean lithospheric mantle

were intercalated with the dominant Proterozoic lithospheric mantle during Siberian craton assembly. Most likely, the Archaean domains (including eclogites (Pearson et al., 1995c)) were thrusted into the Proterozoic mantle via complex tectonic displacement of portions of the lithospheric mantle during Paleoproterozoic orogeny or underplating (Liu et al., 2016; Wang et al., 2018). Alternatively, the olivine-rich materials in this study could be recycled fragments of Archean cratonic roots, first delaminated then incorporated in the Proterozoic lithospheric mantle by upwelling asthenosphere.

5.6. *Not all cratonic mantle is Archean*

Early Re-Os studies of coarse peridotites from cratons in South Africa and North America provided mainly Archean T_{RD} ages (Carlson, 2005; Pearson, 1999) and were seen as evidence that cratonic lithospheric mantle only formed in the Archean. As a result, the terms 'Archean' and 'craton' are often considered essentially synonymous, i.e. the lithospheric mantle in all cratons is presumed to have formed in the Archean. However, data compilations (Doucet et al., 2015; Wittig et al., 2010b) show that a significant proportion of peridotites from the Slave and North Atlantic cratons record T_{RD} ages of 1.8–1.9 Ga matching major crust generation events in those cratons. The central Siberian craton is the first proven case of a craton whose lithospheric mantle formed essentially in the Paleoproterozoic (Ionov et al., 2015b), concomitant with major crust formation or rejuvenation events (Moyen et al., 2017; Paquette et al., 2017). Lithospheric peridotites at the NE margin of the Siberian craton have both Archean and Paleoproterozoic ages (Ionov et al., 2015a) (Fig. 12a).

Recent Re-Os studies of peridotite xenoliths in kimberlites from Arctic Canada have provided other examples of cratons with Paleoproterozoic mantle roots. Liu et al. (2018) reported ~2 Ga T_{RD} ages for peridotites from diamond-bearing kimberlites at the Parry Peninsula and Central Victoria Island, whose mineral and whole rock chemistry is

909 indistinguishable from that of typical cratonic mantle lithosphere. Kimberlite-borne peridotite

910 xenoliths from the central Rae craton (Liu et al., 2016) show both Archean and 2.1–1.7 Ga

911 ages; the Paleoproterozoic peridotites are interpreted to represent juvenile lithospheric mantle

912 that replaced and/or mixed with the lower portion of Archean lithospheric mantle to form

913 thick lithospheric roots extending well into the diamond stability field. Overall, the new data

914 place the final limit for the formation of cratonic lithosphere with specific modal and

915 chemical compositions, and the transition from the 'Archean' to modern tectonic regimes, at

916 2.0 Ga, rather than at the Archean-Proterozoic boundary as is commonly thought. By contrast,

917 we see no robust evidence from appropriate refractory peridotite xenoliths (representative WR

918 samples, undeformed, high-Mg, low Re/Os) to support speculations (Pernet-Fisher et al.,

919 2015) on even younger (Mesoproterozoic) melt extraction ages in the lithospheric mantle of

920 the central Siberian craton (Fig. 12).

921

922 **6. Conclusions**

923 (1) The Udachnaya kimberlite in the central Siberian craton hosts very rare, small fragments

924   of previously unreported coarse and sheared dunites as well as megacrystalline xenoliths

925   (olivine >1–2 cm), equilibrated at 783–1154°C and 3.9–6.5 GPa (~120–220 km).

926 (2) The coarse dunites, olivine megacrysts and low-opx harzburgites have similar bulk

927   variation ranges of Ca, Al, Fe, Cr and Mg# (0.917–0.934) typical of refractory cratonic

928   peridotites, but the dunites and bulk megacrysts have higher MgO, NiO and Mg/Si_{mol}

929   ratios. Modal abundances and those of Ca and Al are not correlated with $Mg\#_{WR}$, and may

930   not be due to differences in melting degrees.

931 (3) Some xenoliths show high $^{187}Re/^{188}Os$ positively correlated with $^{187}Os/^{188}Os$ consistent

932   with the eruption age of host kimberlite (0.37 Ga). The Os depletions and enrichments in

933   Re and other incompatible elements may be linked to fluids related to the generation and

934 fractionation of kimberlite liquids that were coeval with, or operated shortly before, the

935 kimberlite eruption.

936 (4) Robust T_{RD} ages for 16 low-$^{87}Re/^{188}Os$ (0.02–0.13) xenoliths are distinctly lower for

937 harzburgites (1.9–2.1 Ga; average 2.0 ± 0.1 Ga) than for dunites and olivine megacrysts

938 (2.4–3.1 Ga; av. 2.8 ± 0.25 Ga). The dunites and megacrysts define two subsets with

939 average T_{RD} of 2.6 ± 0.1 Ga and 3.0 ± 0.1 Ga, and T_{MA} of 3.0 ± 0.2 Ga and 3.3 ± 0.1 Ga.

940 The difference in grain size (medium- to coarse-grained dunites vs. megacrystalline

941 xenoliths) is not related to age. Thus, the dunites or olivine megacrysts could not be

942 produced by re-melting of harzburgites, nor be melt channel materials in harzburgites.

943 (5) The dunites are relict fragments of lithospheric mantle formed in two Archean events (at

944 or soon after 2.6 and 3.0 Ga) and incorporated into present mantle lithosphere during the

945 final assembly of the Siberian craton in the Paleoproterozoic. These formation ages of the

946 mantle lithosphere are consistent with crustal basement ages from U-Pb dating of zircons.

947 (6) The new data from Siberia and other cratons suggest that the formation of cratonic

948 lithosphere with specific modal and chemical compositions did not stop at the Archean-

949 Proterozoic boundary as is commonly thought, but continued in the Paleoproterozoic.

950

963

964

965   References

966   Abersteiner, A., Kamenetsky, V.S., Goemann, K., Golovin, A.V., Sharygin, I.S., Pearson, D.G.,
967   Kamenetsky, M. and Gornova, M.A. (2019) Polymineralic inclusions in kimberlite-hosted megacrysts:
968   Implications for kimberlite melt evolution. Lithos 336-337, 310-325.

969   Abersteiner, A., Kamenetsky, V.S., Golovin, A.V., Kamenetsky, M. and Goemann, K. (2018) Was
970   crustal contamination Involved in the formation of the serpentine-Free Udachnaya-East kimberlite?
971   New insights into parental melts, liquidus assemblage and effects of alteration. Journal of Petrology
972   59, 1467-1492.

973   Agashev, A.M., Ionov, D.A., Pokhilenko, N.P., Golovin, A.V., Cherepanova, Y. and Sharygin, I.S.
974   (2013) Metasomatism in lithospheric mantle roots: Constraints from whole-rock and mineral chemical
975   composition of deformed peridotite xenoliths from kimberlite pipe Udachnaya. Lithos 160–161, 201-
976   215.

977   Aulbach, S., Mungall, J.E. and Pearson, D.G. (2016) Distribution and Processing of Highly
978   Siderophile Elements in Cratonic Mantle Lithosphere. Reviews in Mineralogy & Geochemistry 81,
979   239-304.

980   Bascou, J., Doucet, L.S., Saumet, S., Ionov, D.A., Ashchepkov, I.V. and Golovin, A.V. (2011)
981   Seismic velocities, anisotropy and deformation in Siberian cratonic mantle: EBSD data on xenoliths
982   from the Udachnaya kimberlite. Earth and Planetary Science Letters 304, 71-84.

983   Batanova, V.G., Thompson, J.M., Danyushevsky, L.V., Portnyagin, M.V., Garbe-Schönberg, D.,
984   Hauri, E., Kimura, J.-I., Chang, Q., Senda, R., Goemann, K., Chauvel, C., Campillo, S., Ionov, D.A.
985   and Sobolev, A.V. (2019) New Olivine Reference Material for In Situ Microanalysis. Geostandards
986   and Geoanalytical Research 43, 453-473.

987   Becker, H., Horan, M.F., Walker, R.J., Gao, S., Lorand, J.P. and Rudnick, R.L. (2006) Highly
988   siderophile element composition of the Earth's primitive upper mantle: Constraints from new data on
989   peridotite massifs and xenoliths. Geochimica et Cosmochimica Acta 70, 4528-4550.

990   Bernstein, S., Hanghoj, K., Kelemen, P. and Brooks, C. (2006) Ultra-depleted, shallow cratonic
991   mantle beneath West Greenland: dunitic xenoliths from Ubekendt Ejland. Contributions to Mineralogy
992   and Petrology 152, 335-347.

993   Boyd, F.R., Pokhilenko, N.P., Pearson, D.G., Mertzman, S.A., Sobolev, N.V. and Finger, L.W.

994   (1997) Composition of the Siberian cratonic mantle: evidence from Udachnaya peridotite xenoliths.

995   Contributions to Mineralogy and Petrology 128, 228-246.

996   Brenan, J.M. and Andrews, D. (2001) High-temperature stability of laurite and Ru-Os-Ir alloy and

997   their role in PGE fractionation in mafic magmas. Can. Mineral. 39, 341-360.

998   Brey, G.P. and Köhler, T. (1990) Geothermobarometry in four-phase lherzolites II. New

999   thermobarometers, and practical assessment of existing thermobarometers. Journal of Petrology 31,

1000   1353-1378.

1001   Burton, K.W., Schiano, P., Birck, J.-L., Allegre, C.J., Rehkämper, M., Halliday, A.N. and Dawson,

1002   J.B. (2000) The distribution and behaviour of rhenium and osmium amongst mantle minerals and the

1003   age of the lithospheric mantle beneath Tanzania. Earth Planet Sci Lett 183, 93-106.

1004   Carlson, R.W. (2005) Application of the Pt–Re–Os isotopic systems to mantle geochemistry and

1005   geochronology. Lithos 82, 249-272.

1006   Carlson, R.W., Pearson, D.G., Boyd, F.R., Shirey, S.B., Irvine, G., Menzies, A.H. and Gurney, J.J.

1007   (1999) Re-Os systematics of lithosphere peridotites: implications for lithosphere formation and

1008   preservation, in: Gurney, J.J., Gurney, J.L., Pascoe, M.D., Richardson, S.H. (Eds.), Proc. 7th Internatl.

1009   Kimberlite Conf. RedRoof Design, Cape Town, pp. 99-108.

1010   Carlson, R.W., Pearson, D.G. and James, D.E. (2005) Physical, chemical, and chronological

1011   characteristics of continental mantle. Reviews of Geophysics 43, RG1001.

1012   Condie, K.C. (2014) Growth of continental crust: a balance between preservation and recycling.

1013   Mineralogical Magazine 78, 623–637.

1014   Doucet, L.S., Ionov, D.A. and Golovin, A.V. (2013) The origin of coarse garnet peridotites in

1015   cratonic lithosphere: new data on xenoliths from the Udachnaya kimberlite, central Siberia.

1016   Contributions to Mineralogy and Petrology 165, 1225-1242.

1017   Doucet, L.S., Ionov, D.A. and Golovin, A.V. (2015) Paleoproterozoic formation age for the

1018   Siberian cratonic mantle: Hf and Nd isotope data on refractory peridotite xenoliths from the

1019   Udachnaya kimberlite. Chem Geol 391, 42-55.

1020   Doucet, L.S., Ionov, D.A., Golovin, A.V. and Pokhilenko, N.P. (2012) Depth, degrees and tectonic

1021   settings of mantle melting during craton formation: inferences from major and trace element

1022   compositions of spinel harzburgite xenoliths from the Udachnaya kimberlite, central Siberia. Earth

1023   and Planetary Science Letters 359–360, 206-218.

1024   Doucet, L.S., Mattielli, N., Ionov, D.A., Debouge, W. and Golovin, A.V. (2016) Zn isotopic

1025   heterogeneity in the mantle: A melting control? Earth and Planetary Science Letters 451, 232–240.

1026   Doucet, L.S., Peslier, A.H., Ionov, D.A., Brandon, A.D., Golovin, A.V., Goncharov, A.G. and

1027   Ashchepkov, I.V. (2014) High water contents in the Siberian cratonic mantle linked to metasomatism:

1028   An FTIR study of Udachnaya peridotite xenoliths. Geochimica et Cosmochimica Acta 137, 159-187.

1029   Golovin, A.V., Sharygin, I.S., Kamenetsky, V.S., Korsakov, A.V. and Yaxley, G.M. (2018) Alkali-

1030 carbonate melts from the base of cratonic lithospheric mantle: Links to kimberlites. Chem Geol 483,

1031 261-274.

1032 Golovin, A.V., Sharygin, I.S., Korsakov, A.V., Kamenetsky, V.S. and Abersteiner, A. (2019) Can

1033 primitive kimberlite melts be alkali-carbonate liquids: Composition of the melt snapshots preserved in

1034 deepest mantle xenoliths. Journal of Raman Spectroscopy, 1-19, doi:10.1002/jrs.5701.

1035 Goncharov, A.G., Ionov, D.A., Doucet, L.S. and Pokhilenko, L.N. (2012) Thermal state, oxygen

1036 fugacity and C-O-H fluid speciation in cratonic lithospheric mantle: new data on peridotite xenoliths

1037 from the Udachnaya kimberlite, Siberia. Earth and Planetary Science Letters 357-358, 99-110.

1038 Herzberg, C. (2004) Geodynamic information in peridotite petrology. Journal of Petrology 45,

1039 2507-2530.

1040 Herzberg, C., Condie, K. and Korenaga, J. (2010) Thermal history of the Earth and its petrological

1041 expression. Earth and Planetary Science Letters 292, 79-88.

1042 Herzberg, C. and Rudnick, R. (2012) Formation of cratonic lithosphere: An integrated thermal and

1043 petrological model. Lithos 149, 4-15.

1044 Ionov, D.A. (1998) Trace element composition of mantle-derived carbonates and coexisting phases

1045 in peridotite xenoliths from alkali basalts. Journal of Petrology 39, 1931-1941.

1046 Ionov, D.A., Ashchepkov, I. and Jagoutz, E. (2005) The provenance of fertile off-craton

1047 lithospheric mantle: Sr-Nd isotope and chemical composition of garnet and spinel peridotite xenoliths

1048 from Vitim, Siberia. Chem Geol 217, 41-75.

1049 Ionov, D.A., Carlson, R.W., Doucet, L.S., Golovin, A.V. and Oleinikov, O.B. (2015a) The age and

1050 history of the lithospheric mantle of the Siberian craton: Re–Os and PGE study of peridotite xenoliths

1051 from the Obnazhennaya kimberlite. Earth and Planetary Science Letters 428, 108-119.

1052 Ionov, D.A., Doucet, L.S. and Ashchepkov, I.V. (2010) Composition of the lithospheric mantle in

1053 the Siberian craton: new constraints from fresh peridotites in the Udachnaya-East kimberlite. Journal

1054 of Petrology 51, 2177-2210.

1055 Ionov, D.A., Doucet, L.S., Carlson, R.W., Golovin, A.V. and Korsakov, A.V. (2015b) Post-

1056 Archean formation of the lithospheric mantle in the central Siberian craton: Re–Os and PGE study of

1057 peridotite xenoliths from the Udachnaya kimberlite. Geochimica et Cosmochimica Acta 165, 466-483.

1058 Ionov, D.A., Doucet, L.S., Carlson, R.W., Golovin, A.V. and Oleinikov, O.B. (2018a) Lost in

1059 interpretation: Facts and misconceptions about the mantle of the Siberian craton. A comment on:

1060 "Composition of the lithospheric mantle in the northern part of Siberian craton: Constraints from

1061 peridotites in the Obnazhennaya kimberlite" by Sun et al. (2017). Lithos 314-315, 683-687.

1062 Ionov, D.A., Doucet, L.S., Pogge von Strandmann, P.A.E., Golovin, A.V. and Korsakov, A.V.

1063 (2017) Links between deformation, chemical enrichments and Li-isotope compositions in the

1064 lithospheric mantle of the central Siberian craton. Chem Geol 475, 105-121.

1065 Ionov, D.A., Doucet, L.S., Xu, Y., Golovin, A.V. and Oleinikov, O.B. (2018b) Reworking of

1066 Archean mantle in the NE Siberian craton by carbonatite and silicate melt metasomatism: Evidence

1067 from a carbonate-bearing, dunite-to-websterite xenolith suite from the Obnazhennaya kimberlite.

1068 Geochimica et Cosmochimica Acta 224, 132-153.

1069 Ionov, D.A. and Hofmann, A.W. (2007) Depth of formation of sub-continental off-craton

1070 peridotites. Earth and Planetary Science Letters 261, 620-634.

1071 Ionov, D.A., Savoyant, L. and Dupuy, C. (1992) Application of the ICP-MS technique to trace

1072 element analysis of peridotites and their minerals. Geostandards Newsletter 16, 311-315.

1073 Irvine, G.J., Pearson, D.G., Kjarsgaard, B.A., Carlson, R.W., Kopylova, M.G. and Dreibus, G.

1074 (2003) A Re-Os isotope and PGE study of kimberlite-derived peridotite xenoliths from Somerset

1075 Island and a comparison to the Slave and Kaapvaal cratons. Lithos 71, 461-488.

1076 Ishikawa, A., Senda, R., Suzuki, K., Dale, C.W. and Meisel, T. (2014) Re-evaluating digestion

1077 methods for highly siderophile element and 187Os isotope analysis: Evidence from geological

1078 reference materials. Chem Geol 384, 27-46.

1079 Jean, M.M., Taylor, L.A., Howarth, G.H., Peslier, A.H., Fedele, L., Bodnar, R.J., Guan, Y.,

1080 Doucet, L.S., Ionov, D.A., Logvinova, A.M., Golovin, A.V. and Sobolev, N.V. (2016) Olivine

1081 inclusions in Siberian diamonds and mantle xenoliths: Contrasting water and trace-element contents.

1082 Lithos 265, 31-41.

1083 Kamenetsky, V.S., Golovin, A.V., Maas, R., Giuliani, A., Kamenetsky, M.B. and Weiss, Y. (2014)

1084 Towards a new model for kimberlite petrogenesis: Evidence from unaltered kimberlites and mantle

1085 minerals. Earth-Science Reviews 139, 145-167.

1086 Kamenetsky, V.S., Kamenetsky, M.B., Golovin, A.V., Sharygin, V.V. and Maas, R. (2012)

1087 Ultrafresh salty kimberlite of the Udachnaya–East pipe (Yakutia, Russia): A petrological oddity or

1088 fortuitous discovery? Lithos 152, 173-186.

1089 Kamenetsky, V.S., Kamenetsky, M.B., Sobolev, A.V., Golovin, A.V., Demouchy, S., Faure, K.,

1090 Sharygin, V.V. and Kuzmin, D.V. (2008) Olivine in the Udachnaya-East kimberlite (Yakutia, Russia):

1091 Types, compositions and origins. Journal of Petrology 49, 823-839.

1092 Kang, J.-T., Ionov, D.A., Liu, F., Zhang, C.-L., Golovin, A.V., Qin, L.-P., Zhang, Z.-F. and Huang,

1093 F. (2017) Calcium isotopic fractionation in mantle peridotites by melting and metasomatism and Ca

1094 isotope composition of the Bulk Silicate Earth. Earth and Planetary Science Letters 474, 128-137.

1095 Kelemen, P.B., Joyce, D.B., Webster, J.D. and Holloway, J.R. (1990) Reaction between ultramafic

1096 rocks and fractionating basaltic magma. Experimental investigation of reaction between olivine

1097 tholeiite and harzburgite at 1150-1050°C and 5 Kb. J. Petrol. 31, 99-134.

1098 Kinny, P.D., Griffin, B.J., Heaman, L.M., Brakhfogel, F.F. and Spetsius, Z.V. (1997) SHRIMP U-

1099 Pb ages of perovskite from Yakutian kimberlites. Geologiya i Geofizika 38, 91-99 (in Russian).

1100 Kitayama, Y., Thomassot, E., Galy, A., Golovin, A., Korsakov, A., d'Eyrames, E., Assayag, N.,

1101 Bouden, N. and Ionov, D. (2017) Co-magmatic sulfides and sulfates in the Udachnaya-East pipe

1102 (Siberia): A record of the redox state and isotopic composition of sulfur in kimberlites and their

1103 mantle sources. Chem Geol 455, 315-330.

1104   Li, J., Liang, X.-R., Xu, J.-F., Suzuki, K. and Dong, Y.-H. (2010) Simplified technique for the

1105   measurements of Re-Os isotope by multicollector inductively coupled plasma mass spectrometry

1106   (MC-ICP-MS). Geochemical Journal 44, 73-80.

1107   Liu, J., Brin, L.E., Graham Pearson, D., Bretschneider, L., Luguet, A., van Acken, D., Kjarsgaard,

1108   B., Riches, A. and Mišković, A. (2018) Diamondiferous Paleoproterozoic mantle roots beneath Arctic

1109   Canada: A study of mantle xenoliths from Parry Peninsula and Central Victoria Island. Geochimica et

1110   Cosmochimica Acta 239, 284-311.

1111   Liu, J., Riches, A.J.V., Pearson, D.G., Luo, Y., Kienlen, B., Kjarsgaard, B.A., Stachel, T. and

1112   Armstrong, J.P. (2016) Age and evolution of the deep continental root beneath the central Rae craton,

1113   northern Canada. Precambrian Research 272, 168-184.

1114   Luguet, A., Behrens, M., Pearson, D.G., König, S. and Herwartz, D. (2015) Significance of the

1115   whole rock Re–Os ages in cryptically and modally metasomatised cratonic peridotites: Constraints

1116   from HSE–Se–Te systematics. Geochimica et Cosmochimica Acta 164, 441-463.

1117   McDonough, W.F. and Sun, S.-s. (1995) The composition of the Earth. Chem Geol 120, 223-253.

1118   Meisel, T., Walker, R.J., Irving, A.J. and Lorand, J.-P. (2001) Osmium isotopic compositions of

1119   mantle xenoliths: a global perspective. Geochim. Cosmochim. Acta 65, 1311-1323.

1120   Meisel, T., Walker, R.J. and Morgan, J.W. (1996) The osmium isotopic composition of the Earth's

1121   primitive upper mantle. Nature 383, 517-520.

1122   Moyen, J.-F., Paquette, J.L., Ionov, D.A., Gannoun, A., Korsakov, A.V., Golovin, A.V. and Moine,

1123   B.N. (2017) Paleoproterozoic rejuvenation and replacement of Archaean lithosphere: Evidence from

1124   zircon U-Pb dating and Hf isotopes in crustal xenoliths at Udachnaya, Siberian craton. Earth Planet

1125   Sci Lett 457, 149-159.

1126   Nickel, K.G. and Green, D.H. (1985) Empirical geothermobarometry for garnet peridotites and

1127   implications for the nature of the lithosphere, kimberlites and diamonds. Earth and Planetary Science

1128   Letters 73, 158-170.

1129   Nimis, P. and Grütter, H. (2010) Internally consistent geothermometers for garnet peridotites and

1130   pyroxenites. Contributions to Mineralogy and Petrology 159, 411-427.

1131   Nimis, P. and Taylor, W.R. (2000) Single clinopyroxene thermobarometry for garnet peridotites.

1132   Part I. Calibration and testing of a Cr-in-Cpx barometer and an enstatite-in-Cpx thermometer.

1133   Contributions to Mineralogy and Petrology 139, 541-554.

1134   Palme, H. and O'Neill, H.S.C. (2014) Cosmochemical Estimates of Mantle Composition, in:

1135   Carlson, R.W. (Ed.), Treatise on Geochemistry (Second Edition). Elsevier, Oxford, pp. 1-39.

1136   Paquette, J.L., Ionov, D.A., Agashev, A.M., Gannoun, A. and Nikolenko, E.I. (2017) Age,

1137   provenance and Precambrian evolution of the Anabar shield from U-Pb and Lu-Hf isotope data on

1138   detrital zircons, and the history of the northern and central Siberian craton. Precambrian Research 301,

1139   134-144.

1140   Pearson, D.G. (1999) The age of continental roots. Lithos 48, 171-194.

1141   Pearson, D.G., Carlson, R.W., Shirey, S.B., Boyd, F.R. and Nixon, P.H. (1995a) Stabilisation of

1142   Archaen lithospheric mantle: A Re-Os isotope study of peridotite xenoliths from the Kaapvaal craton.

1143   Earth and Planetary Science Letters 134, 341-357.

1144   Pearson, D.G., Irvine, G.J., Ionov, D.A., Boyd, F.R. and Dreibus, G.E. (2004) Re-Os isotope

1145   systematics and platinum group element fractionation during mantle melt extraction: a study of massif

1146   and xenolith peridotite suites. Chem Geol 208, 29-59.

1147   Pearson, D.G., Shirey, S.B., Carlson, R.W., Boyd, F.R., Pokhilenko, N.P. and Shimizu, N. (1995b)

1148   Re-Os, Sm-Nd, and Rb-Sr isotope evidence for thick Archaean lithospheric mantle beneath the

1149   Siberian craton modified by multistage metasomatism. Geochimica et Cosmochimica Acta 59, 959-

1150   977.

1151   Pearson, D.G., Snyder, G.A., Shirey, S.B., Taylor, L.A., Carlson, R.W. and Sobolev, N.V. (1995c)

1152   Archaean Re-Os age for Siberian eclogites and constraints on Archaean tectonics. Nature 374, 711-

1153   713.

1154   Pearson, D.G. and Wittig, N. (2008) Formation of Archaean continental lithosphere and its

1155   diamonds: the root of the problem. J. Geol. Soc. London 165, 895-914.

1156   Pernet-Fisher, J.F., Barry, P.H., Day, J.M.D., Pearson, D.G., Woodland, S., Agashev, A.M.,

1157   Pokhilenko, L.N. and Pokhilenko, N.P. (2019) Heterogeneous kimberlite metasomatism revealed from

1158   a combined He-Os isotope study of Siberian megacrystalline dunite xenoliths. Geochimica et

1159   Cosmochimica Acta 266, 220-236.

1160   Pernet-Fisher, J.F., Howarth, G.H., Pearson, D.G., Woodland, S., Barry, P.H., Pokhilenko, N.P.,

1161   Pokhilenko, L.N., Agashev, A.M. and Taylor, L.A. (2015) Plume impingement on the Siberian

1162   SCLM: Evidence from Re–Os isotope systematics. Lithos 218–219, 141-154.

1163   Pokhilenko, N.P., Pearson, D.G., Boyd, F.R. and Sobolev, N.V. (1991) Megacrystalline dunites:

1164   sources of Siberian diamonds. Carnegie Inst. Washington Yearbook 90, 11-18.

1165   Pokhilenko, N.P., Sobolev, N.V., Boyd, F.R., Pearson, D.G. and Shimizu, N. (1993)

1166   Megacrystalline pyrope peridotites in the lithosphere of the Siberian platform: mineralogy,

1167   geochemical peculiarities and the problem of their origin. Russian Geology and Geophysics 34, 56-67.

1168   Pollack, H.N. and Chapman, D.S. (1977) On the regional variation of heat flow, geotherms and

1169   lithospheric thickness. Tectonophysics 38, 279-296.

1170   Priyatkina, N., Khudoley, A.K., Collins, W.J., Kuznetsov, N.B. and Huang, H.-Q. (2016) Detrital

1171   zircon record of Meso- and Neoproterozoic sedimentary basins in northern part of the Siberian Craton:

1172   Characterizing buried crust of the basement. Precambrian Research 285, 21-38.

1173   Reisberg, L. and Lorand, J.P. (1995) Longevity of sub-continental mantle lithosphere from osmium

1174   isotope systematics in orogenic peridotite massifs. Nature 376, 159-162.

1175   Reisberg, L., Zhi, X., Lorand, J.-P., Wagner, C., Peng, Z. and Zimmermann, C. (2005) Re–Os and

1176   S systematics of spinel peridotite xenoliths from east central China: Evidence for contrasting effects of

1177   melt percolation. Earth Planet Sci Lett 239, 286-308.

1178   Rosen, O.M. (2002) Siberian craton - a fragment of a Paleoproterozoic supercontinent. Russian

1179 Journal of Earth Sciences 4, 103-119.

1180   Rudnick, R.L. and Walker, R.J. (2009) Interpreting ages from Re–Os isotopes in peridotites Lithos

1181 112, Supplement 2, 1083-1095.

1182   Servali, A. and Korenaga, J. (2018) Oceanic origin of continental mantle lithosphere. Geology 46,

1183 1047-1050.

1184   Shimizu, N., Pokhilenko, N.P., Boyd, F.R. and Pearson, D.G. (1997) Geochemical characteristics

1185 of mantle xenoiliths from the Udachnaya kimberlite pipe. Russian Geology and Geophysics 38, 205-

1186 217.

1187   Shirey, S.B. and Walker, R.J. (1998) The Re-Os isotope system in cosmochemistry and high-

1188 temperature geochemistry. Annu. Rev. Earth Planet. Sci. 26, 423-500.

1189   Smoliar, M.I., Walker, R.J. and Morgan, J.W. (1996) Re–Os ages of group IIA, IIIA, IVA, and

1190 IVB iron meteorites. Science 271, 1099– 1102.

1191   Sobolev, N.V., Logvinova, A.M., Zedgenizov, D.A., Pokhilenko, N.P., Malygina, E.V., Kuzmin,

1192 D.V. and Sobolev, A.V. (2009) Petrogenetic significance of minor elements in olivines from diamonds

1193 and peridotite xenoliths from kimberlites of Yakutia Lithos 112, 701-713.

1194   Sobolev, N.V., Pokhilenko, N.V. and Efimova, E.S. (1984) Diamond-bearing peridotite xenoliths

1195 in kimberlite and the problem of the origin of diamonds. Russ. Geol. Geofys. 25, 63-80.

1196   Spetsius, Z.V. and Serenko, V.P. (1990) Composition of the continental upper mantle and lower

1197 crust beneath the Siberian Platform. Nauka, Moscow.

1198   Streckeisen, A. (1976) To each plutonic rock its proper name. Earth Sci. Rev. 12, 1-33.

1199   Takazawa, E., Frey, F.A., Shimizu, N. and Obata, M. (2000) Whole rock compositional variations

1200 in an upper mantle peridotite (Horoman, Hokkaido, Japan): Are they consistent with a partial melting

1201 process. Geochimica et Cosmochimica Acta 64, 695-716.

1202   Taylor, W.R. (1998) An experimental test of some geothermometer and geobarometer formulations

1203 for upper mantle peridotites with application to the thermobarometry of fertile Iherzolite and garnet

1204 websterite. Neues Jahrbuch fur Mineralogie-Abhandlungen 172, 381-408.

1205   Walker, R.J., Carlson, R.W., Shirey, S.B. and Boyd, F.R. (1989) Os, Sr, Nd, and Pb isotope

1206 systematics of southern African peridotite xenoliths: Implications for the chemical evolution of

1207 subcontinental mantle. Geochim. Cosmochim. Acta 53, 1583-1595.

1208   Walker, R.J., Horan, M.F., Morgan, J.W., Becker, H., Grossman, J.N. and Rubin, A.E. (2002a)

1209 Comparative ^{187}Re-^{187}Os systematics of chondrites - Implications regarding early solar system

1210 processes. Geochim. Cosmochim. Acta 66, 4187-4201.

1211   Walker, R.J., Prichard, H.M., Ishiwatari, A. and Pimentel, M. (2002b) The osmium isotopic

1212 composition of convecting upper mantle deduced from ophiolite chromites. Geochim. Cosmochim.

1213 Acta 66, 329-345.

1214   Walter, M.J. (1999) Melting residues of fertile peridotite and the origin of cratonic lithosphere, in:

1215 Fei, Y., Bertka, C.M., Mysen, B.O. (Eds.), Mantle Petrology: Field Observations and High-Pressure

1216 Experimentation. Spec. Publ. Geochem. Soc. No. 6. Geochemical Society, Houston, pp. 225-239.

1217   Walter, M.J. (2003) Melt extraction and compositional variability in mantle lithosphere, in:

1218 Carlson, R.W. (Ed.), Treatise on Geochemistry. Vol. 2. The Mantle and Core. Elsevier, Amsterdam,

1219 pp. 363-394.

1220   Wang, H., van Hunen, J. and Pearson, D.G. (2018) Making Archean cratonic roots by lateral

1221 compression: A two-stage thickening and stabilization model. Tectonophysics 746, 562-571.

1222   Wiggers de Vries, D.F., Pearson, D.G., Bulanova, G.P., Smelov, A.P., Pavlushin, A.D. and Davies,

1223 G.R. (2013) Re–Os dating of sulphide inclusions zonally distributed in single Yakutian diamonds:

1224 Evidence for multiple episodes of Proterozoic formation and protracted timescales of diamond growth.

1225 Geochimica et Cosmochimica Acta 120, 363-394.

1226   Wittig, N., Pearson, D.G., Baker, J.A., Duggen, S. and Hoernle, K. (2010a) A major element, PGE

1227 and Re-Os isotope study of Middle Atlas (Morocco) peridotite xenoliths: Evidence for coupled

1228 introduction of metasomatic sulphides and clinopyroxene. Lithos 115, 15-26.

1229   Wittig, N., Pearson, D.G., Webb, M., Ottley, C.J., Irvine, G.J., Kopylova, M., Jensen, S.M. and

1230 Nowell, G.M. (2008) Origin of cratonic lithospheric mantle roots: A geochemical study of peridotites

1231 from the North Atlantic Craton, West Greenland. Earth and Planetary Science Letters 274, 24-33.

1232   Wittig, N., Webb, M., Pearson, D.G., Dale, C.W., Ottley, C.J., Hutchison, M., Jensen, S.M. and

1233 Luguet, A. (2010b) Formation of the North Atlantic Craton: Timing and mechanisms constrained from

1234 Re-Os isotope and PGE data of peridotite xenoliths from S.W. Greenland. Chem Geol 276, 166-187.

1235   Xia, J., Qin, L., Shen, J., Carlson, R.W., Ionov, D.A. and Mock, T.D. (2017) Chromium isotope

1236 heterogeneity in the mantle. Earth and Planetary Science Letters 464, 103-115.

1237   Zhang, J., Li, J., Long, X., Sun, S., Yin, L. and Dai, M. (2017) Rhenium-Osmium isotope

1238 measurements of geological reference material BIR-1a: Evaluation of homogeneity and implications

1239 for method validation and quality control. Geostandards and Geoanalytical Research 41, 649-658.

1240   Ziberna, L., Nimis, P., Kuzmin, D.V. and Malkovets, V.G. (2016) Error sources in single-

1241 clinopyroxene thermobarometry and a mantle geotherm for the Novinka kimberlite, Yakutia.

1242 American Mineralogist 101, 2222-2232.

1243

1244 **Figure captions**

1245 **Fig. 1.** Photomicrographs of Udachnaya mantle xenoliths in transmitted plane-polarized light.

1246 Abbreviations: Ol, olivine; Op, orthopyroxene; Cp, clinopyroxene; Gar, garnet; Sp, spinel. A-

1247 B: Olivine megacrysts contain inclusions of Op, Sp (B) and Gar. C-F: coarse dunites (Ol ≤1

1248 cm; ≤8% Op); pyroxene, garnet and spinel grains are usually small and interstitial (E-F), but

1249 some samples contain Op-Sp±Cp intergrowths (C; breakdown products of garnet or high-T

1250 Op) and patches enriched in Gar (D; metasomatic products). G-H: low-opx harzburgites (11–

1251 21% Op) with grain size ranging from medium (G) to coarse (H).

1252 **Fig. 2.** Co-variation plots for modal mineral abundances and $Mg\#_{WR}$ ($Mg/(Mg+Fe)_{mol}$ in

1253 whole-rock samples). Abbreviations: Dun, dunite; Hzb, harzburgite; Opx (Op),

1254 orthopyroxene; Cpx, clinopyroxene; Gar, garnet; r^2, linear correlation coefficient. (A) Olivine

1255 and Opx abundances show a robust ($r^2 = 0.94$) linear correlation for all xenolith types, except

1256 megacrysts with high modal garnet. For simplicity, megacrystalline dunite Uv83-13 and

1257 olivine megacrysts are shown as "megacrysts". (B-F) Abundances of garnet and Cpx show

1258 the same variation range (from zero to 5–6%) in coarse dunites and low-Opx harzburgites and

1259 are not correlated (low r^2) with modal olivine or $Mg\#_{WR}$. The absence of robust correlations

1260 of modal abundances with $Mg\#_{WR}$ indicate that they are not caused by melt extraction events,

1261 and are likely due to metasomatism.

1262 **Fig. 3.** Co-variation plots for major and minor oxides (wt. %) and Mg# ($Mg/(Mg+Fe)_{mol}$) in

1263 whole-rock (WR) xenoliths in this study. The concentrations of oxides hosted mainly by the

1264 low-abundance garnet, cpx and oxides (Al_2O_3, CaO, Cr_2O_3) are not correlated with Mg# and

1265 show the same range for coarse dunites and harzburgites; the harzburgites can be

1266 distinguished with $(Mg/Si)_{mol}$ ratios (B) and the concentrations of MgO, NiO and Na_2O (e, f)

1267 that depend on olivine/opx ratios. Olivine megacrysts and megacrystalline dunite Uv83-13

1268 show lower average concentrations of CaO and Al_2O_3 and higher MgO than coarse dunites.

1269 **Fig. 4.** Co-variation plots of Al_2O_3 vs. FeO (A) and SiO_2 (B) in whole-rock (WR) xenoliths in

1270 this study (wt. %). Abbreviations are same as in Fig. 2. Also shown are: primitive mantle

1271 (PM) after McDonough and Sun (1995), and the fields of cratonic peridotite xenoliths

1272 (Doucet et al., 2013), fertile off-craton peridotite xenoliths from Vitim and Tariat in central

1273 Asia (Ionov et al., 2005; Ionov and Hofmann, 2007), and Horoman massif peridotites that are

1274 residues of low-pressure melting of fertile mantle (Takazawa et al., 2000). Colored lines are

1275 experimental melting residues of batch (blue) and polybaric (red) fractional melting of fertile

1276 mantle (Herzberg, 2004). Thick dashed blue lines show 45% of isobaric batch melting; thick

1277 dashed red lines show 38% of polybaric fractional melting.

1278 **Fig. 5.** Co-variation plots for major oxides, Mg# (Mg/(Mg+Fe)$_{mol}$) and Cr# (Cr/(Cr+Al)$_{mol}$) in

1279 minerals and whole-rocks, and mineral abundances. The Mg# for silicates are the highest in

1280 olivine and the lowest in garnet (A). The xenoliths containing much low-Mg# garnet and/or

1281 ilmenite plot off the linear Mg#$_{Ol}$ vs. Mg#$_{WR}$ correlation (B). The abundance of garnet is

1282 proportional to WR Al$_2$O$_3$ (C). Literature data for Cr# in coarse garnet peridotites from

1283 Udachnaya in (D) are from Doucet et al. (2013); samples that plot to the right from the linear

1284 Cr#$_{WR}$ vs. Cr#$_{Gar}$ correlation (defined by the earlier work) contain Cr-spinel.

1285 **Fig. 6.** A plot of pressure vs. temperature (P-T) estimates for peridotites in this study (Table

1286 1). Gar Meg are garnet-bearing megacrysts. Pressure for garnet-free peridotites (smaller

1287 symbols) is fixed at 3.5 GPa for harzburgites and 4 GPa for dunites. Dunites and olivine

1288 megacrysts are equilibrated in a broad P range (hence, do not come from a specific depth

1289 level in the lithosphere) and plot between the 35mW/m^2 and 40mW/m^2 model conductive

1290 geotherms (Pollack and Chapman, 1977). Also shown are graphite/diamond (G/D) stability

1291 boundary and mantle adiabats for Tp=1250°C and 1300°C.

1292 **Fig. 7**. Primitive mantle-normalized (McDonough and Sun, 1995) patterns for the REE

1293 (left column) and lithophile trace elements (right column) in whole-rock (WR) samples in this

1294 study. Blue lines are olivine megacrysts, red lines are coarse dunites, continuous grey lines

1295 are low-opx harzburgites, dashed grey lines are high-opx harzburgites. Dark-grey fields are

1296 for Udachnaya kimberlites (Kamenetsky et al., 2012). Light-grey fields in plots for coarse

1297 dunites outline the data for harzburgites.

1298 **Fig. 8**. (a) Primitive mantle-normalized (McDonough and Sun, 1995) REE patterns for

garnets in this study (blue lines, olivine megacrysts; red lines, coarse dunites; grey lines are low-opx harzburgites, dashed grey line is garnet 565-10 low in LREE-MREE. Fields in (B-C) outline the data for olivine megacrysts.

Fig. 9. Primitive mantle-normalized patterns for PGE (Becker et al., 2006) and Re (Meisel et al., 2001) in olivine megacrysts (A), coarse dunites (B) and low-opx harzburgites (C) in this study. Dashed lines in (B) and (C) are for peridotites with low Os (<0.04 ppb) and/or high Re (≥0.3 ppb).

Fig. 10. Plots of $^{187}Os/^{188}Os$ vs. $^{187}Re/^{188}Os$ for samples in this study. (A) Taken together (except for sheared dunite 48-12), the 23 xenoliths define a positive linear correlation with a slope corresponding to an age of 0.37 ± 0.12 Ga (2σ), identical to the eruption age of host kimberlite, and initial $^{187}Os/^{188}Os = 0.1127 \pm 0.0026$. Sample 48-12 with aberrantly high $^{187}Os/^{188}Os$ (0.44) and $^{187}Re/^{188}Os$ (40.7) values plots close to the extension of this isochron trend. (B) Harzburgites show higher $^{187}Os/^{188}Os$ ratios than dunites and megacrysts in the subset of xenoliths that show no Os depletions and/or Re enrichments. The four olivine megacrysts and megacrystalline dunite 83-13 define an 'isochron' (green line) with an apparent 2.7 ± 1.2 Ga age and an 0.1069 ± 0.0017 initial, but the uncertainty of this estimate is too high, and the data are too few, to argue that these samples have a common origin or differ in age from coarse dunites.

Fig. 11. Plots of olivine (A) and orthopyroxene (B) abundances vs. model Re-depletion Os isotope ages (T_{RD}) for appropriate xenoliths in this study (excepting those with ≤0.04 ppb Os). The T_{RD} ages are calculated relative to primitive mantle (PM): $^{187}Os/^{188}Os = 0.1296$ (Meisel et al., 2001), $^{187}Re/^{188}Os = 0.4353$ (Becker et al., 2006) and $\lambda^{187}Re = 1.666 \times 10^{-11}$ a^{-1} (Smoliar et al., 1996). Re-enriched samples (Re/Os close to or higher than in PM, hence uncertain T_{RD}) are shown as empty symbols. Continuous straight lines show linear correlations of the robust T_{RD} values (samples with low Re/Os) with modal abundances for individual rock types: (i)
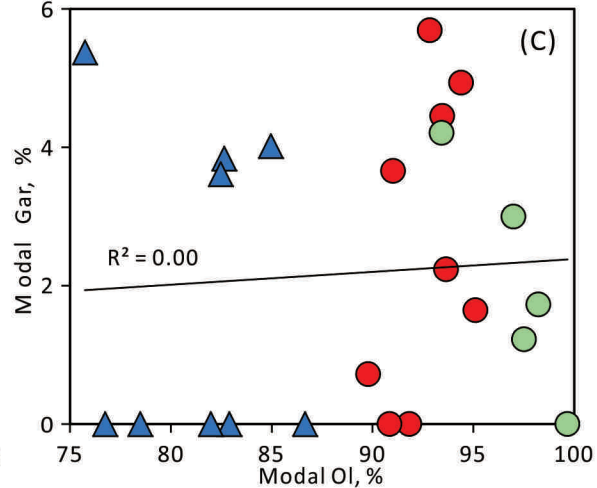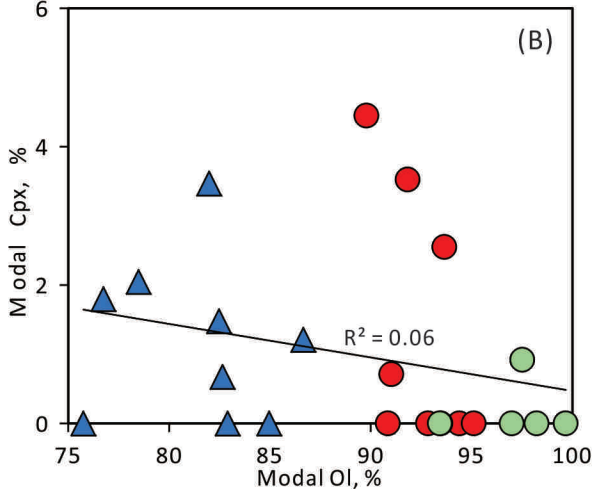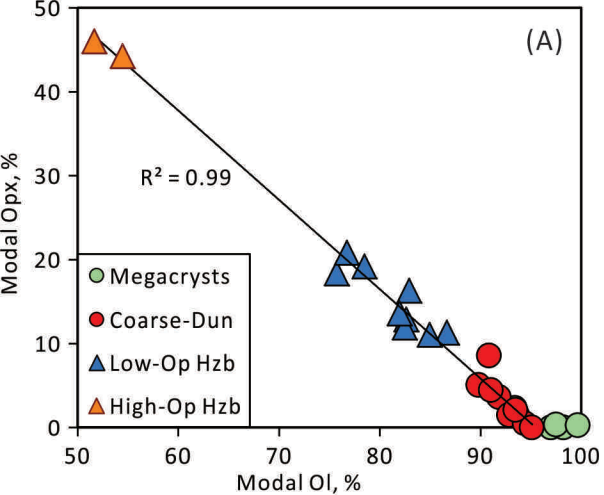
harzburgites (triangles) and (ii) dunites (red circles) grouped with olivine megacrysts (green

circles). Thin dashed lines show linear correlations of the T_{RD} with modal abundances for all

the xenoliths. The T_{RD} seem to be correlated with modal olivine and opx when all the

xenoliths are treated as a single statistical sample (correlation factors r^2 ~0.6–0.7). However,

these seeming correlations are artefacts of combining distinct xenolith types in a single

statistical population because the T_{RD} show opposite correlation trends for individual rock

types (or no correlation, with r^2 close to zero, if samples with high Re/Os are included).

Overall, the plots reflect bimodal age distribution: Paleoproterozoic for harzburgites and

mainly Archean for dunites and olivine megacrysts. This observation, together with the lack

of correlation of the modal abundances with Mg# (Fig. 2 D-F) confirms that the T_{RD} are not

controlled by gradual differences in modal and chemical compositions or melting degrees.
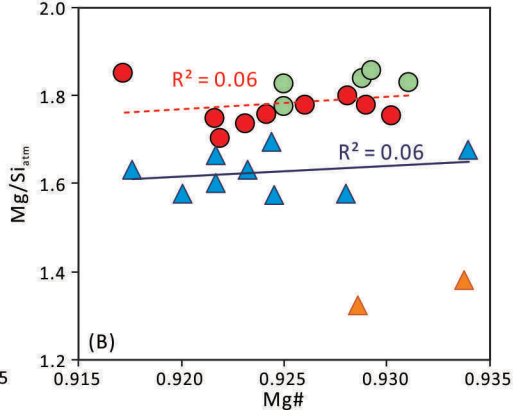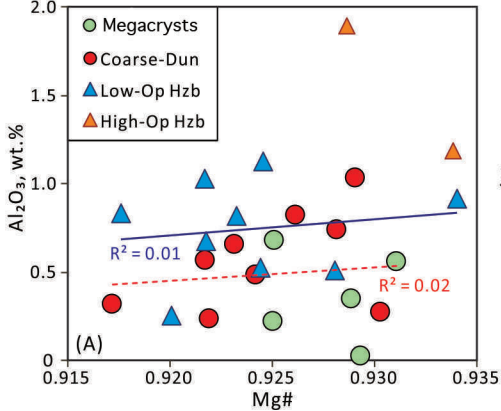
Fig. 12. Cumulative probability distribution (Gaussian plots) for Re-depletion Os isotope

ages (T_{RD}) of mantle xenoliths from the Siberian craton (A) and for U-Pb ages of zircons from

its Precambrian crustal basement (B). (A) The T_{RD} ages for xenoliths in this study (except Os-

depleted and/or Re-enriched samples): red, coarse dunites; green, olivine megacrysts; blue,

low-opx harzburgites. Also shown are literature data for peridotite xenoliths from Udachnaya

(Ionov et al., 2015b) and Obnazhennaya (Ionov et al., 2015a), and for high-Mg# olivine

megacrysts from Udachnaya (Pearson et al., 1995b; Pernet-Fisher et al., 2019) re-calculated

with the PM BSE model (dotted line). The lines are obtained by summing the probability

distributions of a suite of data with normally-distributed errors. T_{RD} uncertainties (standard

deviation, σ) are calculated using the error transfer function; the peak widths are scaled by the

uncertainty of each analysis. The T_{RD} uncertainties of 2σ are used for the Udachnaya data and

of 4σ for the Obnazhennaya data to smooth the plots. (B) Combined U-Pb age data for zircons

from crustal xenoliths (n = 487) in the Udachnaya kimberlite (Moyen et al., 2017), detrital

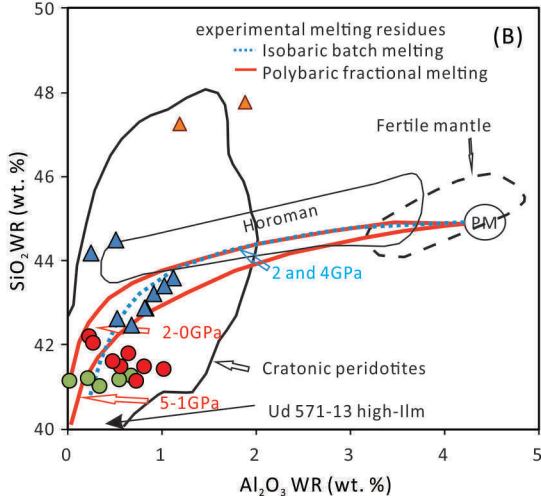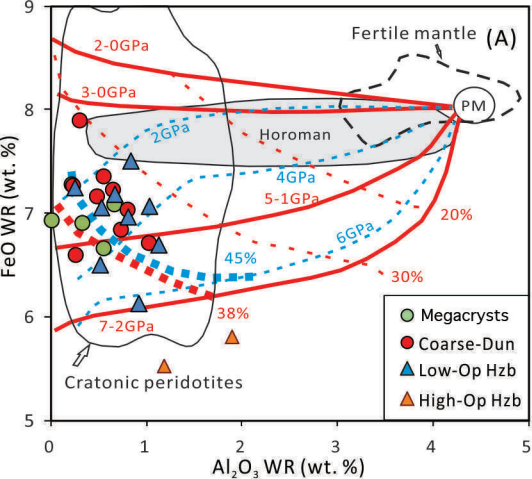zircons from the Anabar shield (n = 479) north of Udachnaya (Paquette et al., 2017) and from

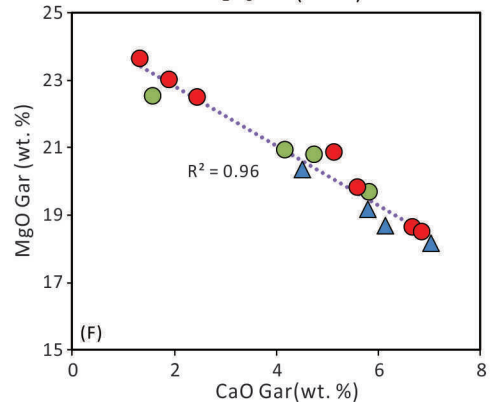1349   nearby Meso- and Neoproterozoic sediments (n = 814) (Priyatkina et al., 2016).
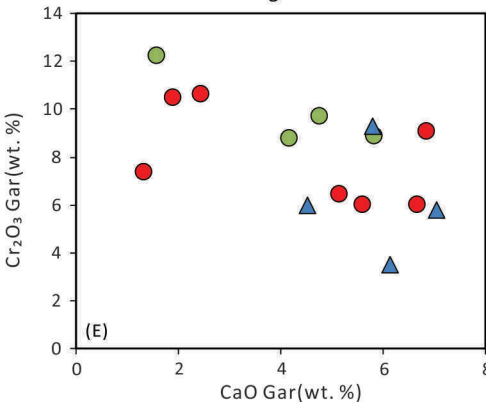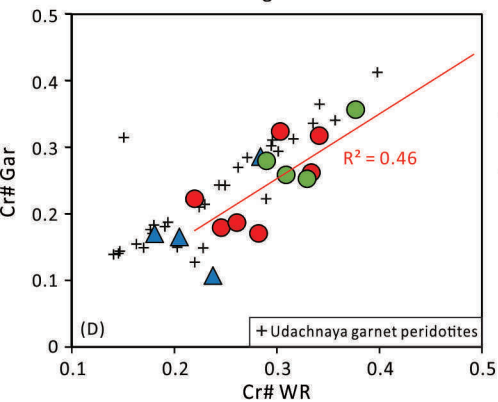
1350

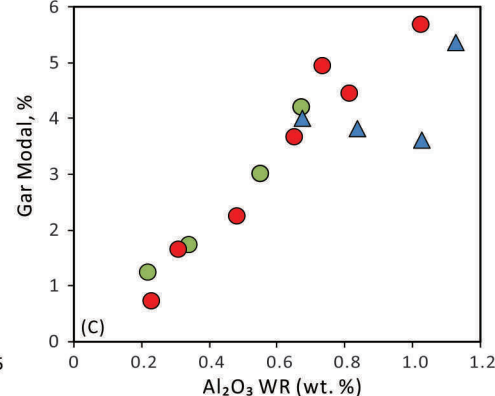(A) Uv6-17 — Megacryst — Ol, Ol — 1 cm

(B) U220 — Megacryst — Ol, Op — 1 cm

(C) Uv499-09 — Coarse dunite — Op, Sp, Op, Ol, Sp, Op, Op — 1 cm

(D) Uv591-09 — Coarse dunite — Gar, Op, Ol — 1 cm

(E) Uv529-10 — Coarse dunite — Ol, Ol — 1 cm

(F) Uv86-13 — Coarse dunite — Ol, Ol — 1 cm

(G) Uv565-10 — Low-Opx Harzburgite — Gar, Gar, Ol, Op — 1 cm

(H) Uv519-13 — Low-Opx Harzburgite — Op, Sp, Cp, Ol, Ol, Op, Sp — 1 cm

Figure A and B: Geochemical plots of FeO WR and SiO₂ WR versus Al₂O₃ WR for peridotite samples.

Figure (A) Megacrysts; (B) Coarse dunites; (C) Low-Opx harzburgites. Y-axis: Garnet/PM. X-axis: La, Ce, Pr, Nd, Sm, Eu, Gd, Tb, Dy, Ho, Er, Tm, Yb, Lu. Labels: 575-13, Meg-Dun n=4, 565-10.

(A) Megacrysts

(B) Coarse dunites
Re-enriched dunites

(C) Low-Opx harzburgites
Re-enriched harzburgties
Low-Os harzburgite

(A) Age=0.37 Ga
Initial $^{187}Os/^{188}Os$=0.1129

Legend:
- Megacrysts
- Coarse-Dun
- Low-Op Hzb
- High-Op Hzb
- Pyroxenite

(B) $R^2 = 0.1$
$R^2 = 0.95$
Age = 2.7±1.2 Ga
Initial $^{187}Os/^{188}Os$=0.1069

Table 1. Summary of petrologic data for samples in this study

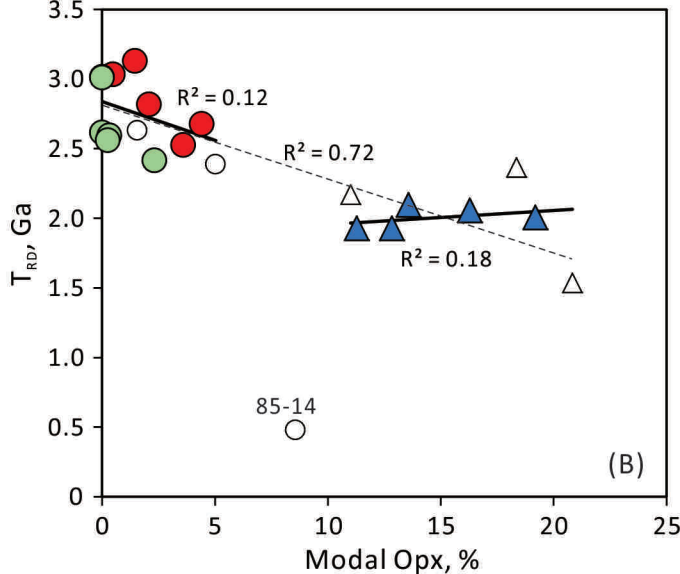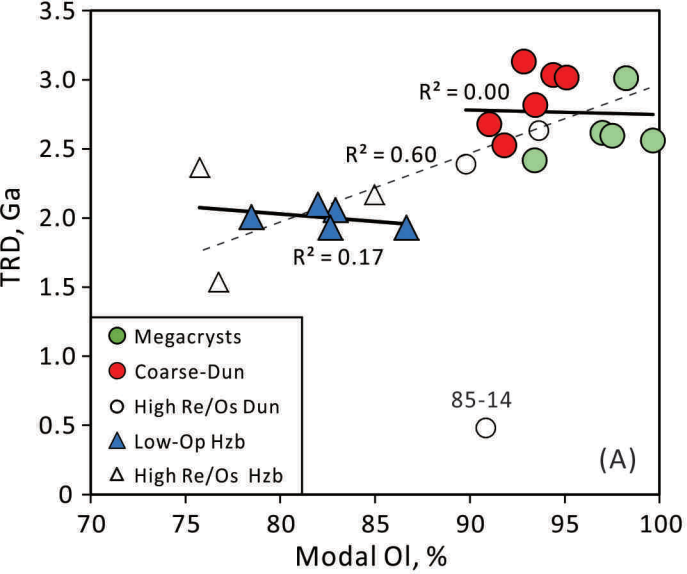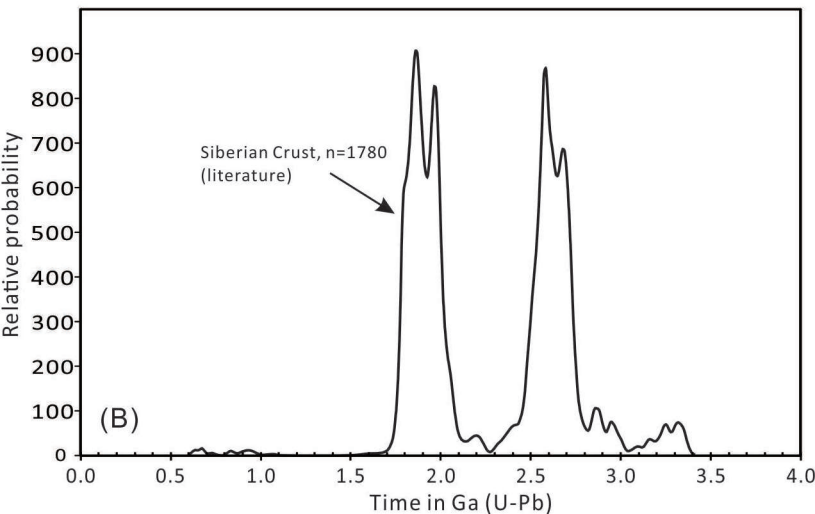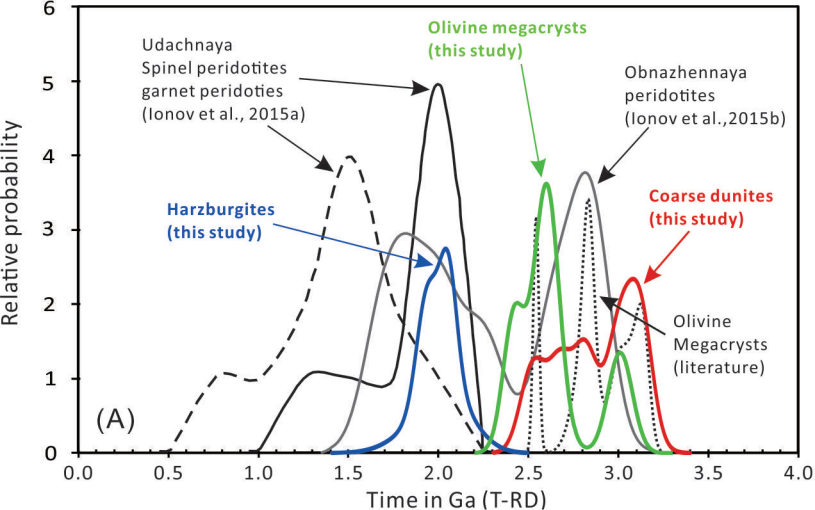| Sample number	WR g	P GPa	T °C	WR composition, wt.%			Mg# Ol	Cr# Spl	Modal composition					
				Al_2O_3	CaO	Mg#	Ol	Spl	Ol	Opx	Cpx	Gar	Spl	Ilm
Olivine megacrysts, and megacrystalline dunite Uv83-13														
U220	93	6.5	1154[d]	0.68	0.47	0.925	0.927	0.90	93	2.3	-	4.2	0.04	-
Uv95-03	71	-	-	0.34	0.21	0.929	0.928	0.86	98	-	-	1.7	0.03	-
Uv83-13	34	-	-	0.55	0.20	0.931	0.933	-	97	-	-	3.0	-	-
Uv569-13	32	4.9	1000[c]	0.22	0.25	0.925	0.926	-	98	0.3	0.9	1.2	-	-
Uv06-17	68	-	-	0.02	0.13	0.929	0.929	0.89	100	0.3	-	-	0.08	-
Averages				*0.36*	*0.25*	*0.928*	*0.929*	*0.88*	*97*	*0.6*		*2.0*		
Coarse dunites														
Uv499-09	93	(4.0)	1028[a]	0.56	0.83	0.922	0.924	0.48	92	3.6	3.5	-	1.0	-
Uv591-09	134	4.0	958[a]	0.23	1.04	0.922	0.923	-	90	5.0	4.4	0.7	-	-
Uv529-10	145	5.4	999[c]	0.66	0.44	0.923	0.926	0.85	91	4.4	0.7	3.7	0.2	-
Uv86-13	145	3.9	946[a]	0.48	0.65	0.924	0.924	-	94	1.6	2.5	2.2	-	-
Uv250-13	71	6.1	1130[d]	1.03	0.28	0.929	0.931	-	93	1.5	-	5.7	-	-
Uv308-13	144	5.2	996[d]	0.74	0.51	0.928	0.934	0.89	94	0.5	-	4.9	0.2	-
Uv571-13	16	-	-	0.31	0.62	0.917	0.932	-	95	-	-	1.6	-	3.2
Uv575-13	63	4.6	783[c]	0.82	0.36	0.926	0.929	-	93	2.1	-	4.5	-	-
Uv85-14	116	(4.0)	857[c]	0.27	0.31	0.930	0.933	0.64	91	8.6	-	-	0.6	-
Averages				*0.57*	*0.56*	*0.925*	*0.928*	*0.71*	*93*	*3.0*	*1.2*	*2.6*		
Sheared dunite														
Uv48-12	44	-	-	0.09	0.48	0.869	0.867	-	99	-	0.5	-	-	-
Low-opx harzburgites														
Uv542-09	142	(3.5)	842[c]	0.9	0.3	0.934	0.934	0.30	83	16	-	-	0.8	-
Uv615-09	77	3.7	857[d]	1.13	1.10	0.925	0.927	0.78	76	18	-	5.4	0.3	0.2
Uv565-10	247	4.2	986[a]	0.84	0.50	0.918	0.921	-	83	13	0.7	3.8	-	-
Uv586-10	124	(3.5)	918[c]	0.25	0.55	0.920	0.920	0.71	78	19	2.0	-	0.3	-
Uv149-11	78	(3.5)	893[c]	0.51	0.52	0.928	0.928	0.56	77	21	1.8	-	0.6	-
Uv44-12	147	(3.5)	977[a]	1.03	0.57	0.922	0.925	0.67	82	12	1.5	3.6	0.5	-
Uv03-13	177	(3.5)	947[c]	0.52	0.35	0.924	0.924	0.47	87	11	1.2	-	0.9	-
Uv63-13	195	5.1	975[d]	0.7	0.8	0.922	0.922	-	85	11	-	4.0	-	-
Uv519-13	215	(3.5)	943[a]	0.82	0.87	0.923	0.929	0.40	82	14	3.5	-	1.0	-
Averages				*0.74*	*0.62*	*0.924*	*0.926*	*0.56*	*81*	*15*	*1.2*	*1.9*	*0.49*	
Opx-rich harzburgites														
Uv101-11	109	(3.5)	961[b]	1.89	0.91	0.929	0.928	0.28	52	46	1.9	-	0.3	-
Uv76-13	223	(3.5)	903[c]	1.19	0.42	0.934	0.933	0.52	55	44	-	-	1.2	-
Averages				*1.54*	*0.66*	*0.931*	*0.931*	*0.40*	*53*	*45*			*0.8*	
Olivine orthopyroxenite														
Uv194-13	120	(2.5)	798[c]	1.82	0.64	0.931	0.931	0.54	21	77	-	-	1.2	-

WR, whole rock (the mass of xenolith material crushed to obtain WR samples is provided). Modal compositions are given normalized to 100% (see text). Ol, olivine; Opx, orthopyroxene; Cpx, clinopyroxene; Gar, garnet; Spl, spinel; Ilm, ilmenite; P, pressure (GPa); T, temperature (°C). Pressure estimated with Opx-Gar method of *Nickel and Green (1985);* values for garnet-free rocks (in parentheses) estimated using P values for samples with similar T's (3.5 or 4.0 GPa). Mineral pairs and methods used for temperature estimates: (a) Cpx-Opx (Taylor, 1998); (b) Ca-in-Cpx (Nimis and Taylor, 2000); (c) Ca-in-Opx (Brey and Kohler, 1990) corrected as in Nimis and Grutter (2010); (d) Opx-Gar (Nimis and Grutter, 2010).

Table 2. Abundances of PGE and Re, $^{187}Re/^{188}Os$ and $^{187}Os/^{188}Os$ ratios, and model age estimates.

N°S	Mg# wr	Al$_2$O$_3$ wr, %	Os ppb	Ir ppb	Ru ppb	Pt ppb	Pd ppb	Re ppb	$^{187}Re/^{188}Os$	$^{187}Os/^{188}Os$	$^{187}Os/^{188}Os$ 0.36 Ga	$^{PM}T_{RD}$ Ga	$^{PM}T_{MA}$ Ga	$^{ch}T_{RD}$ Ga	$^{ch}T_{MA}$ Ga
Olivine megacrysts and megacrystalline dunite															
U220	0.925	0.68	7.9	5.0	11.1	7.9	5.6	0.22	0.133	0.11252	0.11172	2.4	3.3	2.3	3.2
Uv95-03	0.929	0.34	6.9	7.6	11.3	6.3	1.3	0.03	0.019	0.10734	0.10723	3.0	3.1	2.9	3.0
Uv83-13	0.931	0.55	3.5	3.6	11.1	2.3	2.1	0.05	0.074	0.11067	0.11023	2.6	3.1	2.5	3.0
Uv569-13	0.925	0.22	15.8	5.0	10.0	9.5	5.0	0.24	0.074	0.11083	0.11038	2.6	3.0	2.5	2.9
Uv06-17	0.929	0.02	7.6	6.1	16.9	7.9	6.6	0.14	0.090	0.11118	0.11064	2.6	3.1	2.5	3.0
Averages	*0.928*	*0.36*	*8.3*	*5.5*	*12.1*	*6.8*	*4.1*	*0.14*				*2.6*	*3.1*	*2.5*	*3.0*
Coarse dunites															
Uv499-09	0.922	0.56	8.6	3.8	7.3	2.5	2.2	0.07	0.038	0.11113	0.11090	2.5	2.7	2.4	2.6
Uv591-09*	0.922	0.23	0.4	7.6	11.0	0.3	0.3	0.30	3.815	0.13489	0.11194	(2.4)	0.1	(2.3)	
Uv529-10	0.923	0.66	1.8	2.4	1.5	0.8	0.3	0.02	0.054	0.11007	0.10975	2.7	3.0	2.6	2.9
Uv86-13*	0.924	0.48	2.2	2.2	9.8	0.9	0.6	0.35	0.749	0.11461	0.11010	(2.6)		(2.5)	
Uv250-13	0.929	1.03	6.3	5.0	4.6	2.4	0.9	0.07	0.054	0.10663	0.10630	3.1	3.5	3.0	3.4
Uv308-13	0.928	0.74	5.0	3.0	9.5	1.9	2.2	0.04	0.039	0.10727	0.10704	3.0	3.3	2.9	3.2
Uv571-13	0.917	0.31	5.9	n.d.	n.d.	n.d.	n.d.	0.07	0.056	0.10752	0.10719	3.0	3.4	2.9	3.3
Uv575-13	0.926	0.82	3.5	14.4	15.8	13.0	7.7	0.05	0.071	0.10912	0.10869	2.8	3.3	2.7	3.2
Uv85-14**	0.930	0.27	4.3	3.0	8.6	2.0	2.6	0.22	0.244	0.12758	0.12611	(0.5)	0.6	(0.5)	
Averages	*0.925*	*0.57*	*4.2*	*5.2*	*8.5*	*3.0*	*2.1*	*0.13*				*2.8*	*3.2*	*2.8*	*3.1*
Sheared dunite															
*Uv48-12**	*0.869*	*0.09*	*0.02*	*0.03*	*0.27*	*0.25*	*0.30*	*0.15*	*40.7*	*0.4398*	*0.19480*				
Low-opx harzburgites															
Uv542-09	0.934	0.92	4.0	4.0	5.6	0.3	0.3	0.02	0.024	0.11457	0.11443	2.1	2.2	1.9	2.0
Uv615-09*	0.925	1.13	3.7	3.9	7.2	0.9	0.4	0.68	0.879	0.11739	0.11211	(2.4)		(2.2)	
Uv565-10	0.918	0.84	3.3	3.7	11.6	2.0	2.7	0.02	0.025	0.11553	0.11539	1.9	2.0	1.8	1.9
Uv586-10	0.920	0.25	4.3	9.7	14.5	10.4	0.8	0.11	0.126	0.11556	0.11480	2.0	2.7	1.9	2.5
Uv149-11*	0.928	0.51	3.6	3.9	12.2	1.5	2.1	0.39	0.527	0.12149	0.11832	(1.5)		(1.3)	
*Uv44-12**	*0.922*	*1.03*	*0.03*	*0.21*	*0.55*	*0.15*	*0.25*	*0.01*	*1.22*	*0.12423*	*0.11690*	*(1.7)*		*(1.5)*	
Uv03-13	0.869	0.09	2.7	2.7	0.9	1.0	0.5	0.02	0.044	0.11565	0.11539	1.9	2.1	1.8	2.0
Uv63-13*	0.922	0.68	0.7	1.2	0.2	0.2	0.4	0.68	4.75	0.14219	0.11359	(2.2)	0.2	(2.0)	
Uv519-13	0.923	0.82	7.5	4.2	12.4	0.1	0.3	0.08	0.053	0.11446	0.11414	2.1	2.3	2.0	2.2
Averages	*0.918*	*0.70*	*3.7*	*3.7*	*7.2*	*1.8*	*0.9*	*0.22*				*2.0*	*2.3*	*1.9*	*2.1*
Opx-rich harzburgites															
*Uv101-11**	*0.929*	*1.89*	*0.04*	*0.34*	*2.24*	*0.14*	*0.46*	*0.01*	*1.305*	*0.12295*	*0.11510*	*2.0*		*(2.0)*	
*Uv76-13**	*0.934*	*1.19*	*0.01*	*0.03*	*2.08*	*0.09*	*0.30*	*0.04*	*23.66*	*0.2600*	*0.11764*	*1.6*	*0.3*	*(1.6)*	
Olivine orthopyroxenite															
Uv194-13	0.931	1.82	2.3	4.8	25.4	39.7	2.5	0.08	0.168	0.12865	0.12764				

$^{187}Os/^{188}Os$ (0.36 Ga) values are recalculated to the eruption age of the host kimberlite (0.36 Ga) using the ^{187}Re decay constant ($\lambda^{187}Re$) of

1.666 ± 0.005 × 10^{-11} a^{-1} (Smoliar et al. 1996).

$^{PM}T_{RD}$ and $^{PM}T_{MA}$ calculated with PM estimates after Meisel et al. (2001): $^{187}Os/^{188}Os$ = 0.1296 and $^{187}Re/^{188}Os$ = 0.4353. n.d., not determined;

$^{ch}T_{RD}$ and $^{ch}T_{MA}$ calculated with averages for ordinary and enstatite chondrites (Walker et al., 2002): $^{187}Os/^{188}Os$ = 0.1282, $^{187}Re/^{188}Os$ = 0.4215.

*Age estimates in parentheses are uncertain due to low Os (≤0.4 ppb) and/or high Re/Os linked to metasomatism before or during eruption.

**Dunite 85-14 has too high $^{187}Os/^{188}Os$ for an ancient melting residue, likely due to later Re enrichment; its T$_{RD}$ and T$_{AM}$ are not meaningful.

Average values for $^{187}Os/^{188}Os$ (0.36 Ga), T$_{RD}$ and T$_{MA}$ disregard samples with low Os and/or high Re/Os, hence uncertain age estimates.

Negative T$_{MA}$ are not shown, they are due to unreasonably high Re/Os in the samples